nature medicine

ARTICLES

https://doi.org/10.1038/s41591-018-0243-z

Dynamic molecular monitoring reveals that SWI–SNF mutations mediate resistance to ibrutinib plus venetoclax in mantle cell lymphoma

Rishu Agarwal[1,2,12], Yih-Chih Chan[1,2,12], Constantine S. Tam[3,4,5], Tane Hunter[1,2], Dane Vassiliadis[1,2], Charis E. Teh[6,7], Rachel Thijssen[6,7], Paul Yeh[1,2,3], Stephen Q. Wong[1], Sarah Ftouni[1], Enid Y. N. Lam[1,2], Mary Ann Anderson[3,6,7], Christiane Pott[8], Omer Gilan[1,2], Charles C. Bell[1,2], Kathy Knezevic[1], Piers Blombery[1,3], Kathleen Rayeroux[9], Adrian Zordan[9], Jason Li[1,2], David C. S. Huang[6,7], Meaghan Wall[5,9,10], John F. Seymour[2,3], Daniel H. D. Gray[6,7], Andrew W. Roberts[3,6,7,11], Mark A. Dawson[1,2,3,11*] and Sarah-Jane Dawson[1,2,11*]

Ibrutinib plus venetoclax is a highly effective combination in mantle cell lymphoma. However, strategies to enable the evaluation of therapeutic response are required. Our prospective analyses of patients within the AIM study revealed genomic profiles that clearly dichotomized responders and nonresponders. Mutations in *ATM* were present in most patients who achieved a complete response, while chromosome 9p21.1–p24.3 loss and/or mutations in components of the SWI–SNF chromatin-remodeling complex were present in all patients with primary resistance and two-thirds of patients with relapsed disease. Circulating tumor DNA analysis revealed that these alterations could be dynamically monitored, providing concurrent information on treatment response and tumor evolution. Functional modeling demonstrated that compromise of the SWI–SNF complex facilitated transcriptional upregulation of *BCL2L1* (*Bcl-xL*) providing a selective advantage against ibrutinib plus venetoclax. Together these data highlight important insights into the molecular basis of therapeutic response and provide a model for real-time assessment of innovative targeted therapies.

Mantle cell lymphoma (MCL) is a B cell malignancy that is often incurable with conventional chemotherapy[1]. Although therapeutic strategies incorporating autologous transplantation and maintenance rituximab have improved the outcome of younger patients with this disease, there remains an urgent need for novel therapeutic strategies[2]. Constitutive B cell receptor signaling (BCR) and overexpression of prosurvival proteins have emerged as important therapeutic targets in MCL[3]. Ibrutinib (an oral covalent Bruton's tyrosine kinase inhibitor) and venetoclax (a BH3 mimetic with high specificity for BCL2)[4] have both shown excellent clinical activity as monotherapy across several advanced B cell malignancies including MCL[5–7], and preclinical evidence of synergy provides a strong rationale for combining these agents[8–11]. We recently reported the results of the AIM phase 2 clinical trial showing that ibrutinib plus venetoclax achieved a 71% complete response (CR) rate in patients with relapsed/refractory MCL or those who were unsuitable for chemotherapy-based initial treatment[12]. The majority of CRs were negative for minimal residual disease (MRD) by flow cytometry and were durable. Despite this success, the disease in over 20% of patients in the study was primary refractory to the combination therapy, and a further 10% relapsed following initial response.

Although the mutational landscape of MCL has been well characterized[13–18], there is limited understanding of the genomic determinants of response to novel therapies in MCL. Mutations in the NF-κB pathway (*CARD11*, *TRAF2*, *TRAF3* and *BIRC3* mutations) have been associated with ibrutinib resistance in MCL. However, mutations in components of the BCR pathway (*BTK* and *PLCG2* mutations) found in ibrutinib-resistant chronic lymphocytic leukemia (CLL) are rarely seen in MCL[17,19–21]. Similarly, molecular mechanisms conferring resistance to venetoclax in B cell malignancies remain uncharacterized in patients[22]. As these transformative therapies are integrated into clinical practice, it is imperative to understand the relationship between the mutational landscape in MCL and response to combination therapy with ibrutinib and venetoclax.

In parallel to understanding the genomic determinants of response to ibrutinib and venetoclax in MCL, there is a growing need for improved real-time methods to monitor these molecular features in the clinic to predict treatment response and identify emerging resistance. The current approach for MRD monitoring involves flow cytometry of the bone marrow and/or allele-specific oligonucleotide polymerase chain reaction (ASO–PCR) to assess patient-specific immunoglobulin heavy chain (IgH)

[1]Peter MacCallum Cancer Centre, Melbourne, Victoria, Australia. [2]Sir Peter MacCallum Department of Oncology, University of Melbourne, Melbourne, Victoria, Australia. [3]Department of Haematology, Royal Melbourne Hospital & Peter MacCallum Cancer Centre, Melbourne, Victoria, Australia. [4]Department of Haematology, St. Vincent's Hospital, Melbourne, Victoria, Australia. [5]Department of Medicine, St. Vincent's Hospital, Melbourne, Victoria, Australia. [6]Walter and Eliza Hall Institute of Medical Research, Melbourne, Victoria, Australia. [7]Department of Medical Biology, University of Melbourne, Melbourne, Victoria, Australia. [8]University Hospital of Schleswig-Holstein, Kiel, Germany. [9]Victorian Cancer Cytogenetics Service, Melbourne, Victoria, Australia. [10]St. Vincent's Institute of Medical Research, Melbourne, Victoria, Australia. [11]Centre for Cancer Research, University of Melbourne, Melbourne, Victoria, Australia. [12]These authors contributed equally: Rishu Agarwal, Yih-Chih Chan. *e-mail: mark.dawson@petermac.org; sarah-jane.dawson@petermac.org

rearrangements[23–25]. However, these strategies do not capture genomic evolution during therapy or disease progression. The analysis of circulating tumor DNA (ctDNA) represents a previously unexplored modality for disease monitoring and clonal tracking in MCL.

Here, we performed an extensive analysis of patients on the AIM study to identify and characterize molecular mechanisms of resistance to the combination of ibrutinib and venetoclax and to explore the role of ctDNA for real-time monitoring of treatment response in MCL.

Results

Genomic analyses of the AIM clinical cohort. The AIM study (NCT02471391) was an investigator-initiated, open-label, single-arm phase 2 clinical trial[12] approved by the Peter MacCallum Cancer Centre research ethics committee. Twenty-four patients with relapsed/refractory MCL ($n=23$) or previously untreated disease but unsuitable for DNA-damaging therapy ($n=1$) were enrolled (Supplementary Table 1). All patients were initially commenced on ibrutinib monotherapy at 560 mg per day. After 4 weeks, venetoclax was added in a weekly ramp-up to 400 mg per day to reduce the risk of tumor lysis syndrome[12]. Serial computed tomography (CT) and/or [^{18}F]fluorodeoxyglucose positron emission tomography (FDG-PET), bone marrow biopsies (BM) and whole blood samples were collected from all enrolled patients at baseline, at weeks 4, 16, 28, 40 and 56 and at the time of disease progression (Supplementary Tables 1 and 2). The primary endpoint of the clinical trial was CR at week 16. For the analyses reported here, responders ($n=18$) were defined as those who achieved PET-confirmed CR or who had sustained response in the absence of an informative PET (patient 02 whose disease was nonevaluable by FDG-PET but who remained progression free at 27 months). Nonresponders ($n=5$) were defined as those in whom disease was primarily refractory to treatment and who did not achieve PET-confirmed CR. One case was nonevaluable for response due to early death unrelated to progression. This patient did not receive venetoclax and died of infection (patient 14).

Fresh or archival tumor tissue was available in all cases at baseline before treatment ($n=24$), and additional tumor biopsies were also performed where possible at disease progression in patients with acquired resistance ($n=2$; lymph node biopsy in patient 07 and pleural biopsy in patient 01). Comprehensive genomic analyses from tumor tissue, using whole-exome sequencing (WES) and/or targeted amplicon sequencing, revealed somatic mutations in all 24 cases (Fig. 1 and Supplementary Tables 1 and 3). The genes most commonly altered included *ATM* (13/24), *TP53* (12/24), *SMARCA4* (4/24), *WHSC1* (*NSD2*) (4/24), *UBR5* (3/24), *MLL2* (*KMT2D*) (3/24), *NOTCH1* (3/24) and *NOTCH2* (3/24).

Despite the small sample size, tumor mutational profiles were clearly different comparing responders and nonresponders to combination therapy with ibrutinib and venetoclax. All cases with *WHSC1*, *UBR5* and *MLL2* mutations demonstrated a response to therapy, as did 12 of 13 cases with an *ATM* alteration. Conversely, *SMARCA4*, *CCND1* and *NOTCH1* alterations were seen exclusively in nonresponders. Response to therapy was not clearly dichotomized by *TP53* mutational status, with 6 of 18 (33%) responders harboring mutations and/or copy number loss at 17p. Despite this finding, it was notable that all nonresponders were *TP53* mutant, in keeping with the known association between TP53 and poor prognosis in this disease (Supplementary Table 4)[26–30]. Interestingly, we observed that mutations in *CARD11* and *BIRC3*, which have been previously implicated in ibrutinib resistance and which modulate NF-κB activation, did not preclude response to the combination of ibrutinib and venetoclax. However, none of the three patients with aberrations in *TRAF2*, an upstream negative regulator of NF-κB signaling, responded. *BTK* and *PLCG2* mutations associated with ibrutinib resistance in CLL[31] were not identified in this cohort. Conventional clinicopathological characteristics such as lactate dehydrogenase, IgH mutational status and MCL international prognostic index (MIPI) score were not able to predict response across the cohort, except Ki-67 ≥ 30%, which was associated with a reduced likelihood of response ($P=0.02$) to treatment (Fig. 1)[12].

In parallel to the mutational analysis, tumor tissue was also subjected to low-coverage whole-genome sequencing (LC-WGS) to comprehensively profile copy number alterations genome-wide across the cohort (Supplementary Fig. 1 and Supplementary Table 2). GISTIC analysis was performed to examine differences in copy number alterations between responders and non-responders (Supplementary Fig. 1a,b)[32]. Notably, four of five nonresponders were found to harbor a deletion of chromosome 9p21.1–24.3, previously described in MCL[33–35], whereas this deletion was only identified in 1 of 18 responders (Fig. 1 and Supplementary Fig. 1a). In three cases, the 9p loss was identified from baseline tumor material (before treatment), while in the final case, the 9p loss was only identified at the time of disease progression but not in the baseline tumor sample (patient 07, who had a 44% reduction in the sum of perpendicular diameters on CT scan at week 16, but then progressed at week 24). The minimally deleted region common to all four cases spanned a large genomic region of 33.4 megabases encompassing several potentially important genes, including *SMARCA2* and *CDKN2A/B* (Supplementary Fig. 1a). Results from the LC-WGS were independently confirmed using fluorescence in situ hybridization (FISH) DNA probes on formalin-fixed paraffin-embedded tissue where available (Supplementary Fig. 1c).

Mutations in the SWI–SNF chromatin-remodeling complex confer resistance to ibrutinib and venetoclax. The genomic characterization of the clinical cohort clearly identified chromosome 9p loss containing *SMARCA2* (4/5), known pathologic mutations or deletions in *ARID2* (3 of 5) and mutations in the helicase domain of *SMARCA4* (3 of 5) in all the patients who failed to respond to combination therapy (Supplementary Fig. 2a). Together, these data highlighted the SWI–SNF chromatin-remodeling complex[36] as a potential major mutational target conferring resistance to venetoclax and ibrutinib. To characterize the consequences of these genomic determinants of treatment failure functionally, we chose the MCL cell line Z-138 to model resistance mechanisms. The Z-138 cells were ideal for this purpose as they contained a *TRAF2* mutation as well as the commonly deleted region of chromosome 9p present in the nonresponding patients. In this background, we layered in loss of function of SMARCA4 using inducible RNA interference (Fig. 2a and Supplementary Fig. 2b,c). Interestingly, SMARCA4 loss only had a marginal influence on sensitivity to ibrutinib and venetoclax monotherapy, which in the case of venetoclax was best seen at higher concentrations (Supplementary Fig. 3a). Notably and consistent with the findings from the AIM clinical trial, the combination of venetoclax and ibrutinib had the most profound effects on the growth and viability of these cells, and it was in this context that loss of SMARCA4 resulted in marked resistance to therapy (Supplementary Fig. 3a–d). These findings are consistent with the fact that chromosome 9p loss and activation of the NF-κB pathways can be, at least transiently, overcome by ibrutinib plus venetoclax (patient 16). Importantly, when SMARCA4 was functionally compromised in these cells, they selectively acquired a major advantage only in the context of therapeutic pressure (Fig. 2b and Supplementary Fig. 3a–c). As Z-138 cells are *TP53* wild type, this resistance to combination therapy was not dependent on TP53 inactivation.

The Z-138 cells have previously been demonstrated to contain mutations in *NOTCH1*, *TRAF2* and *RELA*[13,17], all of which may influence the response to ibrutinib and venetoclax. Therefore, to specifically understand the importance of SMARCA4 in mediating resistance to the combination of ibrutinib with venetoclax we chose a second MCL cell line, Granta-519, which contains mutations in

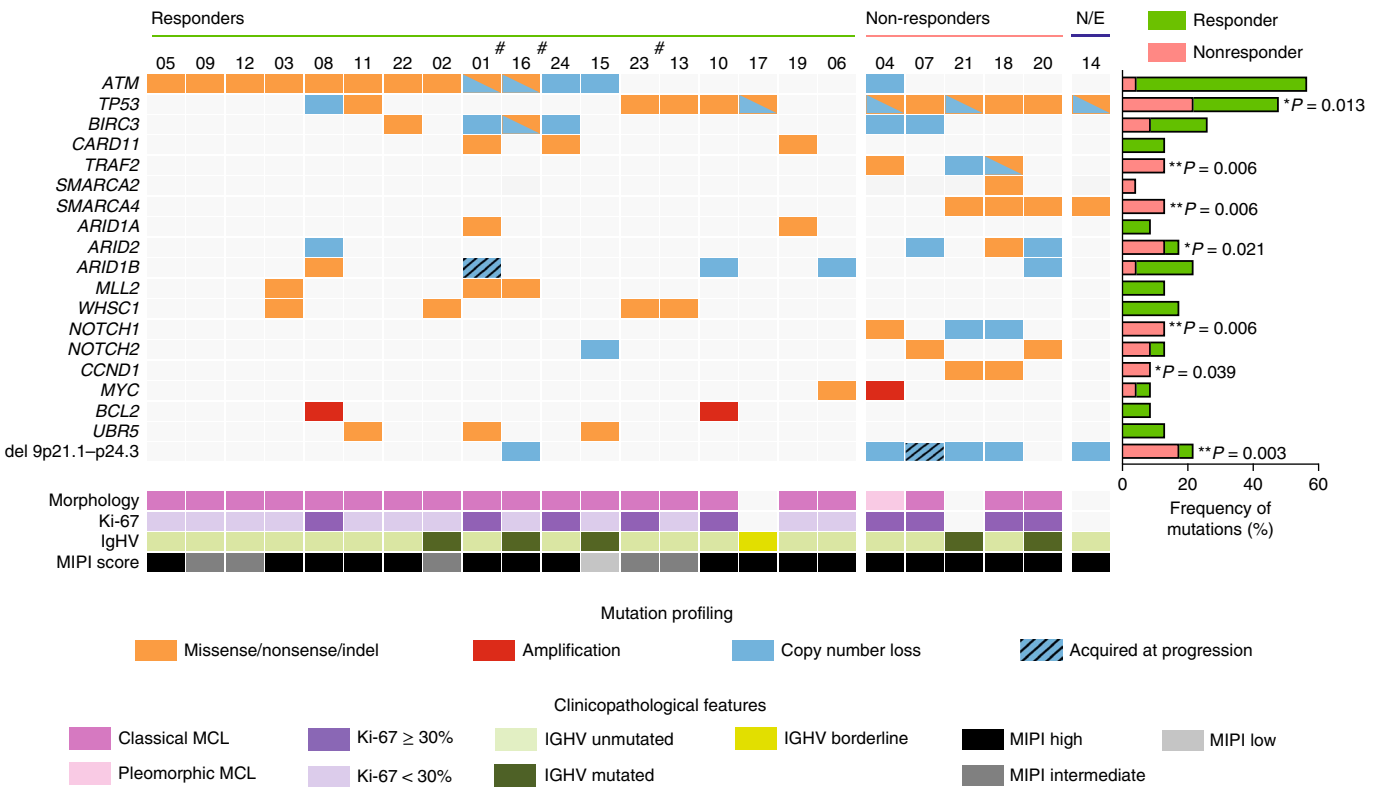

Fig. 1 | Genomic characterization of MCL patients enrolled in the AIM clinical trial. The landscape of somatic mutations detected by WES, targeted amplicon sequencing and LC-WGS of tumor material in the 24 patients enrolled on the AIM trial. Each column represents an individual patient. Patients were divided into responders with clinical remission at week 16 (primary endpoint of the study) and nonresponders who were primarily refractory to the treatment. Three patients (01, 16, 23) who achieved CR relapsed after 56 weeks. One patient (14) who died early was considered N/E (not evaluable). The bar diagrams on the right show the frequency of individual mutations among responders and non-responders. Statistical significance for differences between groups was determined by two-tailed Fisher's exact test; $^{*}P < 0.05$, and $^{**}P < 0.01$. The bottom panel shows clinicopathological parameters assessed for the cohort (morphology, proliferation index for Ki-67, IgH mutation status and MIPI score).

ATM, *MLL2*, *U2AF1* and *WHSC1* but not *NOTCH1* or *TRAF2*[13,17]. The proliferation and viability of Granta-519 cells were also dramatically affected by venetoclax plus ibrutinib (Supplementary Fig. 3e) and, interestingly, knockdown of SMARCA4 alone again resulted in marked resistance to the combination therapy. Together these data highlight the importance of functional compromise of the SWI–SNF chromatin-remodeling complex in mediating resistance to these highly active and potent therapies in MCL.

Therapeutic resistance is mediated by increased Bcl-xL expression. To understand the molecular consequences of SMARCA4 loss we assessed the gene expression changes in Z-138 cells with and without SMARCA4 knockdown before and after combination therapy. Interestingly, the major changes in gene expression were seen with baseline loss of SMARCA4, and combination therapy had very little further influence on gene expression (Supplementary Fig. 3f). Moreover, we found that the marked transcriptional changes observed with loss of SMARCA4 were not associated with any proliferative or survival advantage in the absence of therapeutic pressure (Supplementary Fig. 3c,e). Gene set enrichment analyses did not identify any clear alteration in specific signaling or metabolic pathways. However, assessment of the transcription changes in the antiapoptotic BCL2 family members revealed that Bcl-xL expression was clearly increased following SMARCA4 loss and that cells expressing Bcl-xL were positively selected for with combination therapy (Fig. 2c, Supplementary Fig. 4a,b and Supplementary Table 5). These data were confirmed by quantitative mass cytometry analysis that showed a higher level of Bcl-xL protein after SMARCA4 knockdown that was not further increased by drug treatment (Fig. 2d and Supplementary Fig 4c). Baseline tissue adequate for gene expression analysis was available in seven patients enrolled on the AIM study. Notably, and consistent with our modeling in Z-138 and Granta-519 cells, we found that patients with primary refractory disease containing *SMARCA4* mutations all had a significantly higher baseline expression of Bcl-xL (Fig. 2e and Supplementary Fig. 4d). Together these data suggest that SMARCA4 loss leads to transcriptional changes that prime the cells to survive the therapeutic challenge, and this is reflected in the fact that *SMARCA4* mutations were enriched in patients with primary progression (Fig. 1).

To understand the generalizability of the findings we analyzed a patient who received sequential ibrutinib and venetoclax treatment for relapsed MCL at our institution outside the AIM clinical trial. Genomic analyses at the time of final relapse, when clinically resistant to both ibrutinib and venetoclax, showed that the patient harbored loss of chromosome 9p and also contained a focal deletion of the 5'-end of *SMARCA4* (Fig. 3a,b). Immunohistochemistry of samples taken prior and following resistance to venetoclax showed a dramatic downregulation of BCL2 expression (Fig. 3c). Importantly, the clinically refractory cells that contained loss of chromosome 9p and *SMARCA4* showed a marked increase in Bcl-xL protein levels by western blot (Fig. 3d and Supplementary Fig. 4e) and mass cytometric analysis (Fig. 3e) and were resistant to ibrutinib and venetoclax in vitro (Fig. 4a). These data in a primary patient sample were consistent with the findings from the AIM clinical trial and our functional modeling in MCL cell lines.

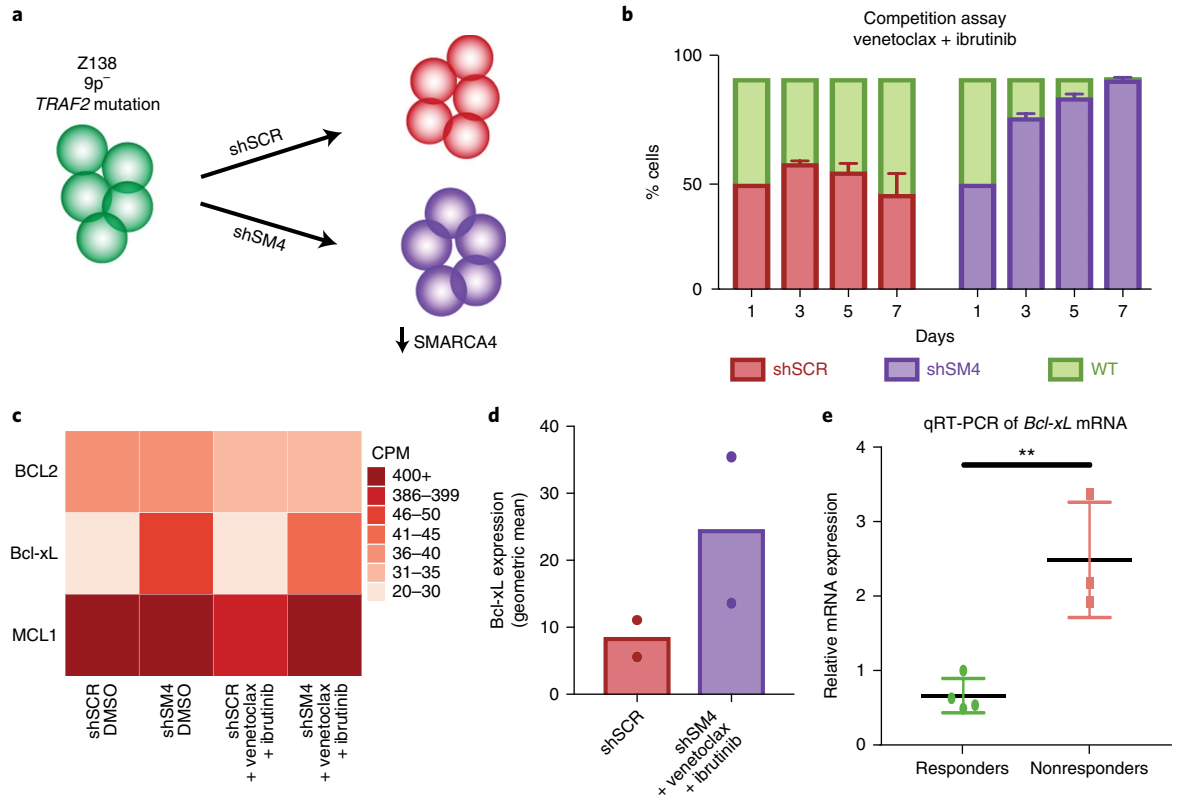

Fig. 2 | Modeling resistance to ibrutinib and venetoclax. a, Shown here is a schematic overview of the experimental plan. Z-138 cells containing chromosome 9p deletion (9p⁻) and *TRAF2* mutation (green) were transduced with an shRNA targeting SMARCA4 (shSM4, purple) or a nonspecific control sequence (shSCR, red). **b**, SMARCA4 knockdown in Z-138 cells provided a survival advantage in the presence of venetoclax (3 μM) and ibrutinib (3 μM). Wild-type Z-138 cells (green) cocultured (1:1) with Z-138 cells containing a control shRNA (red) or an shRNA targeting SMARCA4 (purple) were grown in the presence of venetoclax and ibrutinib and sampled over time. The proportion of the shRNA-expressing cells was determined by flow cytometry. The mean of independent cell culture triplicates is shown. The error bars represent the s.d. **c**, Heatmap comparing the expression levels of BCL2, Bcl-xL and MCL1 in Z-138 cells containing shRNAs with or without combination treatment (8 h). The other BCL2-like proteins, BCLw and BFL1, were not expressed in Z-138 cells. A darker color indicates higher expression. mRNA was collected from the cells on three separate occasions, and expression values shown are the mean. CPM, counts per million. **d**, Mass cytometry analysis performed in duplicate experiments comparing Bcl-xL expression in Z-138 cells containing a control shRNA with shRNA targeting SMARCA4. Graph shows the mean and actual data points. The experiment was independently repeated on three separate occasions. **e**, Bone marrow samples were analyzed for *Bcl-xL* expression. All three nonresponding patients had a *SMARCA4* mutation and showed higher levels of *Bcl-xL* expression than the four responding patients. The graph shows the mean and s.d. of data from the patients in the respective groups. Each data point was performed in technical triplicate. $P = 0.006$ from two-tailed unpaired Student's *t*-test. Please also see Supplementary Fig. 4d for the tumor percentage in each sample.

To understand whether the upregulation of Bcl-xL is a major determinant of resistance to ibrutinib and venetoclax, we treated Z-138 cells in the presence and absence of SMARCA4 loss with the selective Bcl-xL inhibitor A-1331852. Cells with SMARCA4 loss were far more sensitive to Bcl-xL inhibition and, importantly, Bcl-xL inhibition in combination with ibrutinib and venetoclax was able to overcome the resistant phenotype and eradicate these cells (Fig. 4b,c and Supplementary Fig. 4f). These findings were reproduced with navitoclax, a clinically available BH3 mimetic with broader specificity that also inhibits Bcl-xL (Fig. 4d and Supplementary Fig. 4g,h). In addition to these data in MCL cell lines we also assessed the effects of Bcl-xL inhibition in primary cells from the patient who developed resistance to sequential ibrutinib and venetoclax. Consistent with the cell line data, the patient cells containing loss of chromosome 9p and SMARCA4 also showed greater sensitivity to A-1331852 and ABT-737 compared with venetoclax or ibrutinib (Fig. 4a).

Loss of SMARCA4 leads to de-repression of Bcl-xL. We next wanted to gain molecular insights into the mechanism by which loss of SMARCA4 results in increased Bcl-xL expression. As the SWI–SNF complex is known to facilitate chromatin accessibility and the recruitment of transcriptional coactivators to increase transcription, we reasoned that the marked transcriptional changes observed following loss of SMARCA4 would be associated with significant alterations in chromatin accessibility. Consistent with this we found that genes that were repressed following loss of SMARCA4 show decreased chromatin accessibility by assay for transposase-accessible chromatin using sequencing (ATAC-seq) at the cis-regulatory elements adjacent to these genes (Fig. 5a). In contrast, genes that showed increased expression following SMARCA4 loss showed no changes in chromatin accessibility (Fig. 5a). These data suggest that the increased gene expression following SMARCA4 loss is probably indirect via the loss of transcriptional repressors. In accordance with this notion, assessment of the *Bcl-xL* locus confirmed that chromatin accessibility at the cis-regulatory elements was unchanged, but the active enhancer modification H3K27ac at the cis-regulatory elements in *Bcl-xL* was increased following knockdown of SMARCA4 (Fig. 5b,c). Together, these data implied that the increased expression of Bcl-xL was probably driven by a loss of transcriptional repressors at this locus.

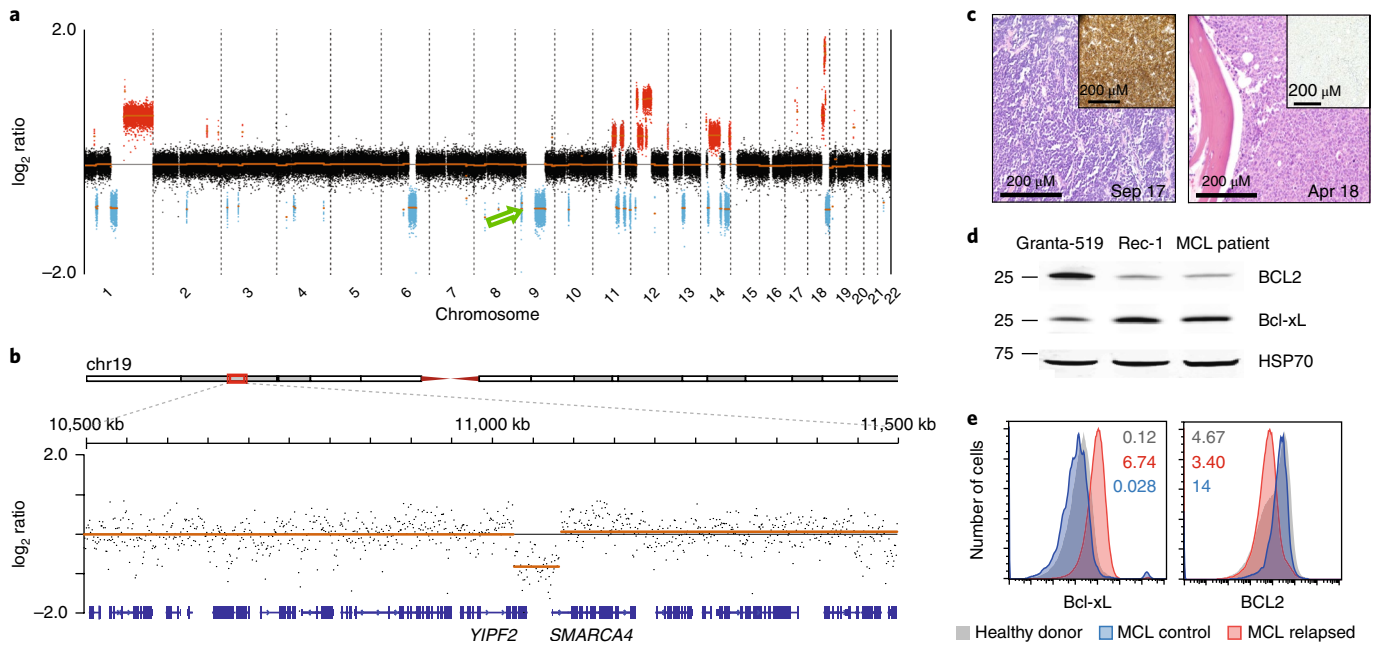

Fig. 3 | Genomic characterization of a non-AIM patient with MCL. a, LC-WGS. The green arrow highlights the heterozygous loss of chromosome 9p. **b**, LC-WGS, showing a region of chromosome 19 encompassing the *SMARCA4* locus. **c**, Tissue biopsy (H&E) with BCL2 immunohistochemistry (inset) prevenetoclax (left) and postvenetoclax (right) showing marked reduction in BCL2 expression with venetoclax therapy. This experiment was performed once as testing was done on patient samples with limited material. **d**, Western blot comparing BCL2 and Bcl-xL expression in primary patient sample and two MCL cell lines. This experiment was performed once as testing was done on patient samples with limited material. **e**, The expression of BCL2 and Bcl-xL measured by mass cytometry analysis of MCL cells isolated from a patient resistant to ibrutinib and venetoclax relative to peripheral blood B cells collected from a normal donor and to another primary MCL sample taken from a patient not exposed to either ibrutinib or venetoclax. This experiment was independently repeated on two separate occasions from the same patient sample.

Although the transcriptional control of the BCL2 family of proteins is not fully understood, recent reports have suggested that the bZIP transcription factor ATF3 is a direct repressor of *Bcl-xL* transcription[37]. Interestingly, we find that loss of SMARCA4 leads to a dramatic reduction in chromatin accessibility at the *ATF3* locus, and this is associated with decreased *ATF3* gene expression (Fig. 5d). To assess the functional role of ATF3 in mediating resistance secondary to SMARCA4 loss we used RNAi to knock down ATF3. This resulted in increased expression of Bcl-xL (Fig. 5e) and remarkably phenocopied the effects of SMARCA4 loss by providing resistance to venetoclax and ibrutinib (Fig. 5f). Together these data provide important insights into the molecular mechanisms by which functional compromise of the SWI–SNF chromatin-remodeling complex mediates resistance to venetoclax and ibrutinib (Fig. 5g). Although *ATF3* is not frequently mutated in MCL these data highlight the importance of understanding the transcriptional control of the BCL2 family of proteins to identify other potential avenues of resistance. Moreover, although ATF3 is a major regulator of Bcl-xL in the cells we have studied, it remains possible that other transcriptional repressors of Bcl-xL may be important in different cellular contexts where these drugs are used as anticancer therapies.

Monitoring treatment response by ctDNA. Having established the genomic determinants of resistance to ibrutinib and venetoclax we next wanted to evaluate how this knowledge might be applied in the clinical setting. We first assessed whether ctDNA analysis could be used to prospectively evaluate treatment response and characterize the molecular changes governing treatment resistance in patients on the AIM study. Plasma DNA from all 24 patients was initially subjected to targeted amplicon sequencing, covering a panel of 42 genes known to be recurrently mutated in MCL (Supplementary Tables 1, 2, 6 and 7). At baseline, before treatment, ctDNA was detected in 17 of 24 individuals (71%). In all of the seven cases where ctDNA was not detected, disease was localized and confined to the lymph nodes (without evidence of bone marrow involvement). Of the 17 cases with detectable ctDNA at baseline, mutant allele fractions ranged from 0.4 to 60% (Supplementary Table 8). Serial samples ($n=91$; median 6 samples per patient) from 16 of 17 cases with detectable ctDNA were available for targeted amplicon sequencing and droplet digital PCR (Supplementary Table 9) to evaluate serial changes in ctDNA levels. ctDNA dynamics closely mirrored treatment responses (Fig. 6a and Supplementary Figs. 5–8). Serial ctDNA collection was not performed for one of the nonresponding patients (patient 21), who had rapid disease progression on ibrutinib.

In parallel to the ctDNA analysis, IgH rearrangements were identified in tumor tissue of 16 of 24 (67%) cases, and serial ASO–PCR analysis was performed on peripheral blood in all 16 individuals. ctDNA and ASO–PCR results were directly compared across 74 serial timepoints where both analyses were performed and showed concordance in 62 of 74 (83.8%) samples (Supplementary Table 10). Serial assessment of BM MRD status by flow cytometry was performed in all 24 individuals. ctDNA and BM MRD results were directly compared across 108 timepoints where both analyses were performed and showed concordance in 92 of 108 (85%) samples (Supplementary Table 11). In five of the discordant timepoints, flow cytometry of BM became transiently positive for low volume disease following the initial 4 weeks of ibrutinib treatment. Serial BM assessment showed subsequent clearance following the addition of venetoclax. In contrast, ctDNA did not show this transient increase, consistent with previous studies where we showed that ctDNA more accurately reflects disease response and is not influenced by the transient redistribution of malignant lymphocytes following ibrutinib treament[38] (Supplementary Figs. 5–8).

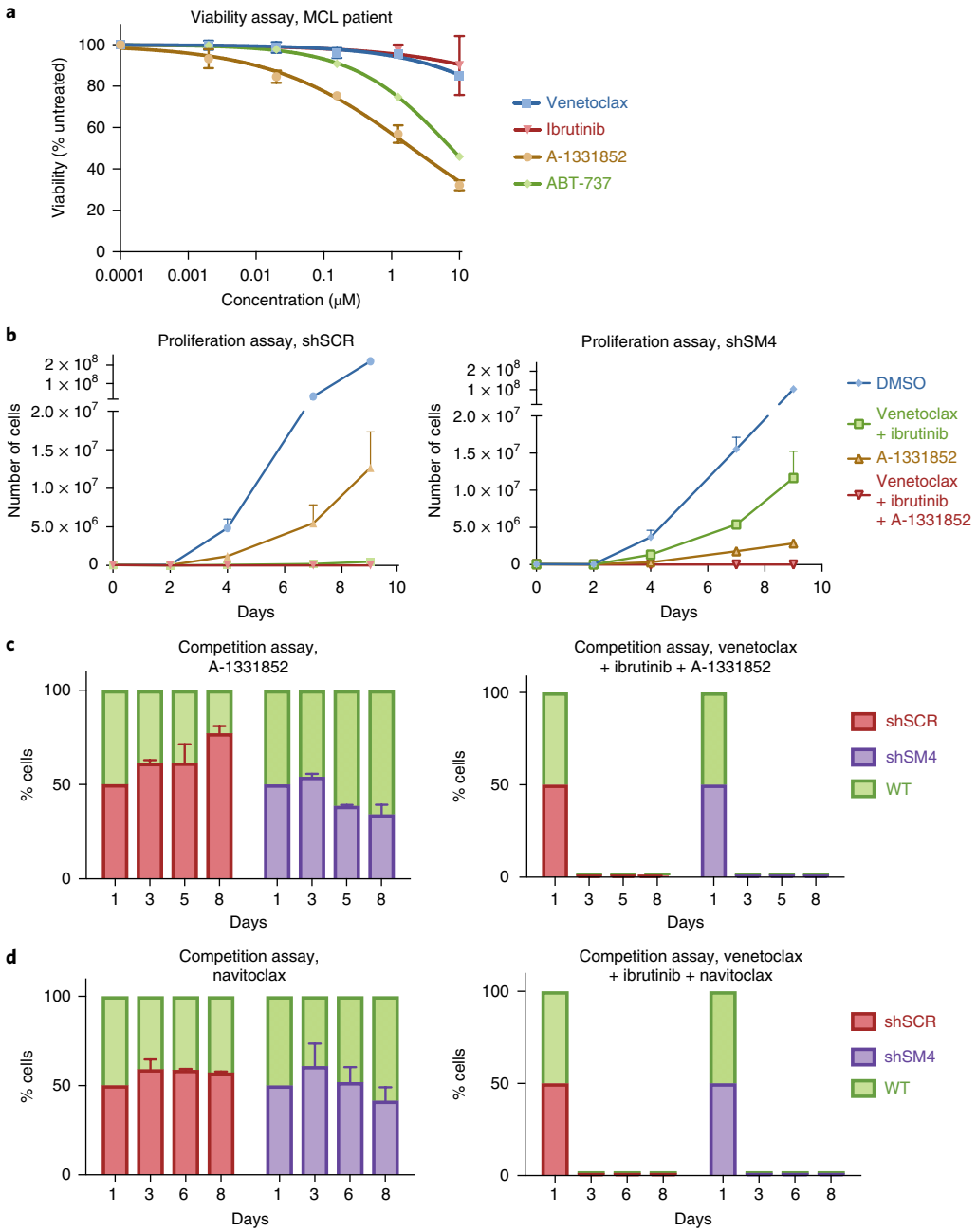

Fig. 4 | Bcl-xL inhibition overcomes ibrutinib and venetoclax resistance. a, Cells from the additional patient whose MCL was resistant to ibrutinib and to venetoclax in vivo were incubated with ibrutinib, venetoclax, ABT-737 and A-1331852 for 24 h. This experiment was performed once as testing was done on patient samples with limited material. **b**, A-1331852 alone more potently inhibited the proliferation of SMARCA4 knockdown cells (right) than shSCR cells (left). In cells with loss of SMARCA4, A-1331852 was able to overcome resistance to venetoclax and ibrutinib when used in combination with these drugs. **c**, Wild-type Z-138 (green) cocultured (1:1) with Z-138 cells containing shRNA control (red) or SMARCA4-targeted shRNA (purple) were grown in the presence of A-1331852 alone (left) or in combination with venetoclax and ibrutinib (right) and sampled over time. The proportion of the different cell types was analyzed by flow cytometry. **d**, Wild-type Z-138 cells (green) cocultured with Z-138 cells containing shRNA control (red) or SMARCA4-targeted shRNA (purple) were grown in the presence of 50 nM navitoclax (left) or a combination of 3 μM venetoclax, 3 μM ibrutinib and 50 nM navitoclax (right) in triplicate and sampled over time. The proportion of the shRNA-expressing cells was determined by flow cytometry. All experiments shown represent the mean and s.d. of three independent cell culture replicates, and this experiment was independently repeated on three separate occasions. Venetoclax (3 μM), ibrutinib (3 μM) and A-1331852 (100 nM) were used (in **b**–**d**) unless otherwise stated.

The achievement of MRD-negative status following treatment was assessed using ctDNA and compared with flow cytometry and ASO–PCR in evaluable patients who (i) had positivity for the MRD marker before the commencement of combination therapy and (ii) had serial samples available for assessment (Fig. 6b). Of the MRD-evaluable patients who achieved CR by imaging, 10 of 11 (91%) achieved MRD-negative status by ctDNA analysis, with a similar proportion becoming negative when assessed by BM flow cytometry (14 of 15 (93%)) and ASO–PCR (9 of 11 (82%)). One individual (patient 23) remained positive by all three assays, despite CR documented on imaging at week 16. However, this patient manifested asymptomatic relapse with progressive disease in the BM

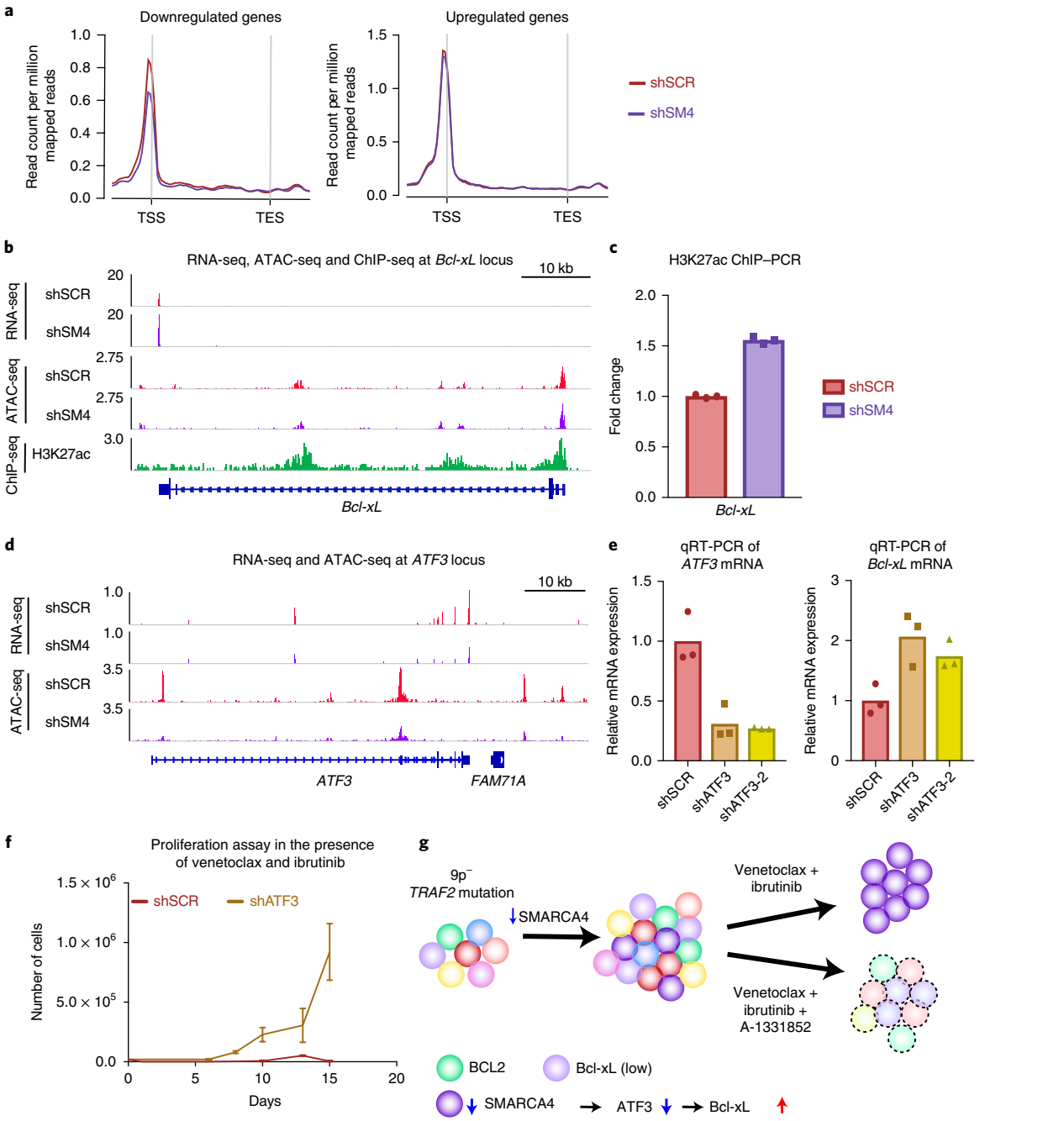

Fig. 5 | SMARCA4 regulates the expression of ATF3. a, Averaged chromatin accessibility derived from ATAC-seq and plotted for genes that were significantly up- and downregulated following SMARCA4 knockdown. TSS, transcriptional start site; TES, transcriptional end site. **b**, Genome browser snapshot of RNA expression level and chromatin accessibility at the *Bcl-xL* locus in control and SMARCA4 knockdown Z-138 cells. H3K27ac ChIP in wild-type Z-138 cells is also shown to highlight enhancer regions. **c**, ChIP–PCR of H3K27ac at an enhancer region in control and SMARCA4 knockdown Z-138 cells. The graph represents the mean of technical triplicates, and this experiment was independently repeated on two separate occasions. **d**, Genome browser snapshot of RNA expression level and chromatin accessibility at the *ATF3* locus in control and SMARCA4 knockdown Z-138 cells. **e**, *ATF3* (left) and *Bcl-xL* (right) mRNA levels in control and ATF3 knockdown Z-138 cells. The graph represents the mean of technical triplicates, and this experiment was independently repeated on three separate occasions. **f**, Proliferation assay of control and ATF3 knockdown Z-138 cells that were cultured in the presence of 3 μM venetoclax and 3 μM ibrutinib. The graph represents the mean and s.d. of three independent cell culture replicates, and this experiment was independently repeated on three separate occasions. **g**, Model of emergence of drug resistance with treatment. A heterogeneous population of MCL cells with loss of chromosome 9p and *TRAF2* mutation expresses varying levels of prosurvival proteins (red, green and purple). On treatment with venetoclax and ibrutinib, a resistant clone with functional compromise of SMARCA4 survives owing to a decreased expression of ATF3 and increased expression of Bcl-xL (dark purple). Combination treatment with venetoclax, ibrutinib and A-1331852 kills the resistant cells.

documented at week 56, which highlights the greater sensitivity of the laboratory assays over imaging assessment. In the final case (patient 17), ASO–PCR has remained positive at very low levels, despite achievement of MRD-negative status by ctDNA and flow cytometric analysis; notably this patient continues to remain in CR at 65 weeks on treatment.

Three patients showed an initial complete response to therapy followed by disease progression (Fig. 6a–c and Supplementary Fig. 7). In these cases, driver mutations identified at baseline in ctDNA showed initial response to therapy with a reduction in mutant allele fractions in plasma and a subsequent rise coincident with disease progression, suggesting failure of treatment to eradicate the dominant clone. Importantly, in patient 16, ctDNA levels began to rise several weeks before recurrent disease was evident by ASO–PCR, BM flow cytometry assessment or radiological imaging (Fig. 6c). Further evidence of the clinical value of ctDNA was demonstrated in patient 01. This case was the only patient with acquired resistance for whom tumor tissue at progression was available. LC-WGS of the tumor tissue at the time of disease progression revealed the acquisition of several new copy number alterations on chromosome 6, including 6p loss. This region encompasses several genes including *ARID1B*, part of the SWI–SNF complex. Notably, LC-WGS of plasma at the time of disease progression revealed that the copy number alterations in the resistant cells could be readily identified from the ctDNA analysis (Supplementary Fig. 8).

Five patients displayed primary resistance to treatment and ctDNA remained detectable at all timepoints (Fig. 6a and Supplementary Fig. 6). Importantly, the ctDNA analysis revealed the ease by which *SMARCA4* mutations could be identified and monitored in these cases using a minimally invasive approach. In parallel to the targeted amplicon sequencing, plasma DNA was also subjected to LC-WGS to understand whether the same copy number alterations identified in the tumor tissue analysis could be detected using ctDNA testing. GISTIC analysis confirmed enrichment of the same chromosome 9p loss in plasma DNA from nonresponders that had been characterized from analysis of the tumor samples (data not shown). In patient 07, the chromosome 9p loss had not been identified in the pretreatment primary tumor sample but was identified from a tumor biopsy taken at the time of disease progression (week 24). Importantly, this copy number alteration was found to emerge in the plasma at 16 weeks, 8 weeks before the identification of progressive disease on imaging (Fig. 6d), further highlighting the utility of ctDNA to monitor disease evolution in real time.

Prognostic value of genomic characteristics and ctDNA. We next explored the relationship between baseline tumor genomic characteristics, ctDNA levels and patient outcomes in this cohort. Patients who harbored either a *SMARCA4* mutation and/or chromosome 9p21.1–p24.3 loss at baseline showed inferior progression-free survival (hazard ratio (HR) = 21, $P=0.00012$) (Fig. 6e, top). Similarly, detection of ctDNA at baseline before treatment (Fig. 6e, bottom) was associated with inferior progression-free survival (HR = 11, $P=0.018$). Presence of *SMARCA4* mutation and/or chromosome 9p21.1–p24.3 loss at baseline and detection of ctDNA at baseline were also associated with inferior time to progression (Supplementary Fig. 9).

Discussion

MCL remains incurable in the vast majority of patients with relapsed and refractory disease. The AIM study has revealed the potential for durable complete remissions in these patients with the combination of ibrutinib and venetoclax[12]. These data are likely to be practice changing and herald a new era of combination targeted therapies for this disease. It is nonetheless important to note that 20% of patients enrolled on this study demonstrated primary resistance to the combination therapy and a further 10% relapsed with acquired resistance. Here we have established the molecular rationale to guide patient selection for this highly effective combination therapy and provide a detailed molecular understanding of the mechanisms of resistance. We highlight the ability of ctDNA to characterize the genomic alterations governing treatment response using a minimally invasive approach. We establish that ctDNA performs at least as well as the existing methods of flow cytometry and ASO–PCR for the measurement of MRD. Beyond quantitative MRD monitoring, ctDNA additionally provides valuable prognostic information and enables real-time assessment of tumor evolution to reveal the emergence of genomic changes associated with treatment resistance.

The baseline genomic characterization revealed mutations in the SWI–SNF chromatin-remodeling complex and/or loss of chromosome 9p in all patients who demonstrated primary resistance to ibrutinib and venetoclax. These genomic features are not infrequent in relapsed MCL and have both predictive and prognostic impact in the context of salvage therapy with ibrutinib and venetoclax. Recurrent deletion of chromosome 9p in MCL was initially described over two decades ago[35]. This region is gene rich with a number of potential oncogenes and tumor suppressors including *JAK2*, *SMARCA2*, *MTAP* and *CDKN2A/B*. Interestingly, homozygous deletions of *CDKN2A/B* have recently been associated with venetoclax resistance in CLL[39]. In our functional analysis Granta-519 cells, which are homozygous null for *CDKN2A/B*, are still responsive to therapy but rapidly acquire resistance when *SMARCA4* is lost. These data suggest that *CDKN2A/B* loss by itself is insufficient to confer resistance in MCL. However, it certainly remains possible that loss of *CDKN2A/B* facilitates resistance to these therapies in the context of impaired SWI/SNF activity.

Fig. 6 | ctDNA analysis allows monitoring of treatment response and emerging resistance in patients treated with ibrutinib and venetoclax. a, Serial analysis of ctDNA levels and treatment responses in patients on treatment. Green lines indicate individual patients who achieved CR, showing that ctDNA was undetectable after 16–28 weeks of treatment. Red lines indicate patients with stable or progressive disease with ctDNA remaining detectable at all time points. Blue lines indicate patients who relapsed after CR with ctDNA levels rising concomitantly with disease progression. The shaded area represents the period of ibrutinib monotherapy between study commencement and the end of week 4. All analyses were performed in duplicate from the same plasma samples. **b**, Assessment of MRD in evaluable patients by ctDNA, BM flow cytometry and peripheral blood ASO-PCR. Yellow boxes represent achievement of MRD-negative status, and pink boxes represent persistent MRD positivity at the time of best response. Gray boxes represent cases that were considered not evaluable for MRD assessment. **c**, The disease kinetics of a relapsing patient (patient 16) assessed using ctDNA analysis, ASO–PCR and radiological imaging. The patient attained CR at 16 weeks and then relapsed with disease progression. Disease relapse was most sensitively detected by ctDNA at 28 weeks with an increase in mutant allele fraction (MAF) for *ATM* and *BIRC3* mutations. In comparison, relapsed disease only became detectable at 40 weeks by ASO–PCR and at 56 weeks by imaging. All analyses were performed in duplicate from the same plasma samples. **d**, Detection of emerging resistance by ctDNA in a patient (patient 07) with disease progression after having stable disease for 16 weeks. Copy number alterations by LC-WGS were compared between tumor biopsies before the start of treatment and at disease progression. The deletion of chromosome 9p21.1–p24.3 was only identified in the progression tumor biopsy. The bottom panel shows LC-WGS plots for plasma samples. The deletion of chromosome 9p21.1–p24.3 was evident on the ctDNA analysis at 16 weeks, which was 8 weeks before the identification of progressive disease by radiological imaging. **e**, Genomic characteristics and ctDNA levels predict patient outcome. Cox proportional hazard analyses at baseline showing that the detection of *SMARCA4* mutations and/or chromosome 9p21.1–p24.3 deletion (top) and the detection of ctDNA (bottom) are associated with inferior progression-free survival. The shaded area represents 95% confidence intervals; survival analyses were performed using the Cox proportional hazards model. For patient groups with no events, Cox regression with Firth's penalized likelihood were used to estimate significance and hazard ratios.

Mutations in the SWI–SNF chromatin-remodeling complex are present in over 20% of human malignancies, and this chromatin complex represents a focal point for somatic mutations that offer cancers a selective advantage[40]. It is still unclear why mutations in the SWI–SNF complex are observed so frequently in cancer[36]. Our data suggest that functional impairment of the SWI–SNF complex in MCL results in marked transcriptional changes that do not selectively influence particular metabolic or signaling pathways. Instead, the transcriptional noise created by functional compromise of SWI–SNF provides the ideal adaptive milieu whereby a population of cells is always present and poised with the right transcriptional program to survive a selective pressure. In our study, impairment of SWI–SNF resulted in the upregulation of Bcl-xL, which is a key survival molecule able to subvert the effects of

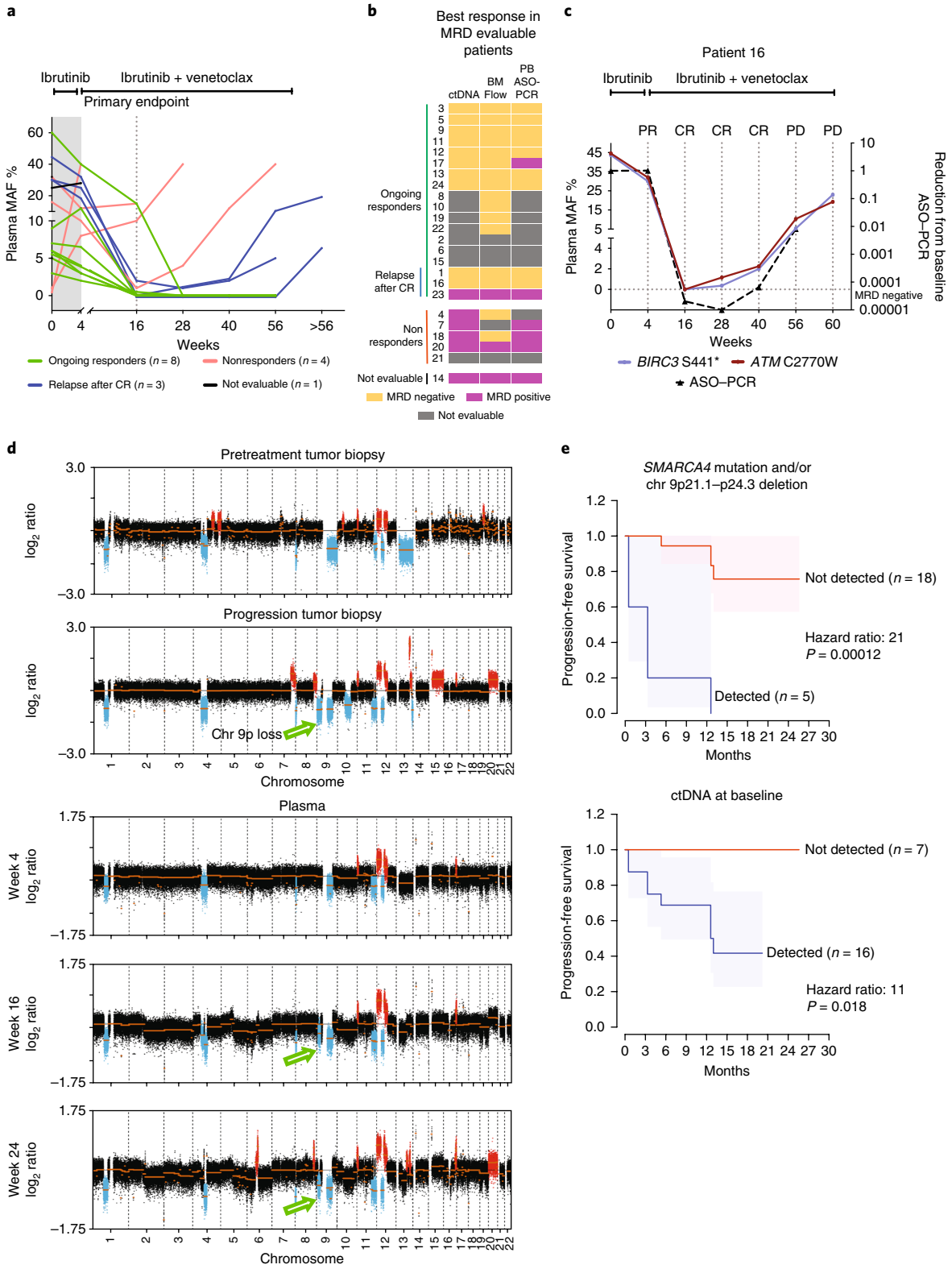

ibrutinib and venetoclax in MCL (Fig. 5g). Although it remains possible that other gene expression changes may contribute to the resistance phenotype, our findings highlight that the increased Bcl-xL expression present in cell lines and patients represents a dominant escape mechanism from the combination of ibrutinib and venetoclax. Importantly, drugs that specifically target Bcl-xL are able to synergize with these therapies to overcome this resistance. These findings generate the prediction that patients with this molecular profile, which can be identified from ctDNA testing, may benefit from broader targeting of the prosurvival proteins; this is a hypothesis that we seek to pursue in clinical trials of novel combination strategies to further improve the outcome for patients with MCL.

Online content

Any methods, additional references, Nature Research reporting summaries, source data, statements of data availability and associated accession codes are available at https://doi.org/10.1038/s41591-018-0243-z.

Received: 9 March 2018; Accepted: 21 September 2018;
Published online: 19 November 2018

References

1. Cheah, C. Y., Seymour, J. F. & Wang, M. L. Mantle cell lymphoma. *J. Clin. Oncol.* **34**, 1256–1269 (2016).
2. Le Gouill, S. et al. Rituximab after autologous stem-cell transplantation in mantle-cell lymphoma. *N. Engl. J. Med.* **377**, 1250–1260 (2017).
3. Martin, P., Ruan, J. & Leonard, J. P. The potential for chemotherapy-free strategies in mantle cell lymphoma. *Blood* **130**, 1881–1888 (2017).
4. Souers, A. J. et al. ABT-199, a potent and selective BCL-2 inhibitor, achieves antitumor activity while sparing platelets. *Nat. Med.* **19**, 202–208 (2013).
5. Wang, M. L. et al. Targeting BTK with ibrutinib in relapsed or refractory mantle-cell lymphoma. *N. Engl. J. Med.* **369**, 507–516 (2013).
6. Davids, M. S. et al. Phase I first-in-human study of venetoclax in patients with relapsed or refractory non-Hodgkin lymphoma. *J. Clin. Oncol.* **35**, 826–833 (2017).
7. Dreyling, M. et al. Ibrutinib versus temsirolimus in patients with relapsed or refractory mantle-cell lymphoma: an international, randomised, open-label, phase 3 study. *Lancet* **387**, 770–778 (2016).
8. Zhao, X. et al. Combination of ibrutinib with ABT-199: synergistic effects on proliferation inhibition and apoptosis in mantle cell lymphoma cells through perturbation of BTK, AKT and BCL2 pathways. *Br. J. Haematol.* **168**, 765–768 (2015).
9. Axelrod, M. et al. Combinatorial drug screening identifies synergistic co-targeting of Bruton's tyrosine kinase and the proteasome in mantle cell lymphoma. *Leukemia* **28**, 407–410 (2014).
10. Li, Y. et al. FBXO10 deficiency and BTK activation upregulate BCL2 expression in mantle cell lymphoma. *Oncogene* **35**, 6223–6234 (2016).
11. Beltran, E. et al. A cyclin-D1 interaction with BAX underlies its oncogenic role and potential as a therapeutic target in mantle cell lymphoma. *Proc. Natl Acad. Sci. USA* **108**, 12461–12466 (2011).
12. Tam, C. S. et al. Ibrutinib plus venetoclax for the treatment of mantle-cell lymphoma. *N. Engl. J. Med.* **378**, 1211–1223 (2018).
13. Bea, S. et al. Landscape of somatic mutations and clonal evolution in mantle cell lymphoma. *Proc. Natl Acad. Sci. USA* **110**, 18250–18255 (2013).
14. Zhang, J. et al. The genomic landscape of mantle cell lymphoma is related to the epigenetically determined chromatin state of normal B cells. *Blood* **123**, 2988–2996 (2014).
15. Kridel, R. et al. Whole transcriptome sequencing reveals recurrent NOTCH1 mutations in mantle cell lymphoma. *Blood* **119**, 1963–1971 (2012).
16. Meissner, B. et al. The E3 ubiquitin ligase UBR5 is recurrently mutated in mantle cell lymphoma. *Blood* **121**, 3161–3164 (2013).
17. Rahal, R. et al. Pharmacological and genomic profiling identifies NF-κ B-targeted treatment strategies for mantle cell lymphoma. *Nat. Med.* **20**, 87–92 (2014).
18. Greiner, T. C. et al. Mutation and genomic deletion status of ataxia telangiectasia mutated (ATM) and p53 confer specific gene expression profiles in mantle cell lymphoma. *Proc. Natl Acad. Sci. USA* **103**, 2352–2357 (2006).
19. Saba, N. S. et al. Pathogenic role of B-cell receptor signaling and canonical NF-κB activation in mantle cell lymphoma. *Blood* **128**, 82–92 (2016).
20. Wu, C. et al. Genetic heterogeneity in primary and relapsed mantle cell lymphomas: impact of recurrent CARD11 mutations. *Oncotarget* **7**, 38180–38190 (2016).
21. Zhao, X. et al. Unification of de novo and acquired ibrutinib resistance in mantle cell lymphoma. *Nat. Commun.* **8**, 14920 (2017).
22. Tahir, S. K. et al. Potential mechanisms of resistance to venetoclax and strategies to circumvent it. *BMC Cancer* **17**, 399 (2017).
23. van der Velden, V. H. et al. Analysis of minimal residual disease by Ig/TCR gene rearrangements: guidelines for interpretation of real-time quantitative PCR data. *Leukemia* **21**, 604–611 (2007).
24. Cheminant, M. et al. Minimal residual disease monitoring by 8-color flow cytometry in mantle cell lymphoma: an EU-MCL and LYSA study. *Haematologica* **101**, 336–345 (2016).
25. Ferrero, S., Dreyling, M. & European Mantle Cell Lymphoma Network. Minimal residual disease in mantle cell lymphoma: are we ready for a personalized treatment approach? *Haematologica* **102**, 1133–1136 (2017).
26. Eskelund, C. W. et al. TP53 mutations identify younger mantle cell lymphoma patients who do not benefit from intensive chemoimmunotherapy. *Blood* **130**, 1903–1910 (2017).
27. Halldorsdottir, A. M. et al. Impact of TP53 mutation and 17p deletion in mantle cell lymphoma. *Leukemia* **25**, 1904–1908 (2011).
28. Nordstrom, L. et al. SOX11 and TP53 add prognostic information to MIPI in a homogenously treated cohort of mantle cell lymphoma–a Nordic Lymphoma Group study. *Br. J. Haematol.* **166**, 98–108 (2014).
29. Delfau-Larue, M. H. et al. High-dose cytarabine does not overcome the adverse prognostic value of CDKN2A and TP53 deletions in mantle cell lymphoma. *Blood* **126**, 604–611 (2015).
30. Aukema, S. M. et al. Expression of TP53 is associated with outcome of MCL independent of MIPI and Ki-67 in trials of the European-MCL Network. *Blood* **131**, 417–420 (2017).
31. Woyach, J. A. et al. Resistance mechanisms for the Bruton's tyrosine kinase inhibitor ibrutinib. *N. Engl. J. Med.* **370**, 2286–2294 (2014).
32. Mermel, C. H. et al. GISTIC2.0 facilitates sensitive and confident localization of the targets of focal somatic copy-number alteration in human cancers. *Genome Biol.* **12**, R41 (2011).
33. Hartmann, E. M. et al. Pathway discovery in mantle cell lymphoma by integrated analysis of high-resolution gene expression and copy number profiling. *Blood* **116**, 953–961 (2010).
34. Salaverria, I. et al. Specific secondary genetic alterations in mantle cell lymphoma provide prognostic information independent of the gene expression-based proliferation signature. *J. Clin. Oncol.* **25**, 1216–1222 (2007).
35. Dreyling, M. H. et al. Alterations of the cyclin D1/p16-pRB pathway in mantle cell lymphoma. *Cancer Res.* **57**, 4608–4614 (1997).
36. Kadoch, C. & Crabtree, G. R. Mammalian SWI/SNF chromatin remodeling complexes and cancer: mechanistic insights gained from human genomics. *Sci. Adv.* **1**, e1500447 (2015).
37. Chueh, A. C. et al. ATF3 repression of BCL-XL determines apoptotic sensitivity to HDAC inhibitors across tumor types. *Clin. Cancer Res.* **23**, 5573–5584 (2017).
38. Yeh, P. et al. Circulating tumour DNA reflects treatment response and clonal evolution in chronic lymphocytic leukaemia. *Nat. Commun.* **8**, 14756 (2017).
39. Herling, C. D. et al. Clonal dynamics towards the development of venetoclax resistance in chronic lymphocytic leukemia. *Nat. Commun.* **9**, 727 (2018).
40. Dawson, M. A. The cancer epigenome: concepts, challenges, and therapeutic opportunities. *Science* **355**, 1147–1152 (2017).

Acknowledgements

The clinical study was funded by Abbvie and Janssen. The work included in this manuscript was funded by the Leukemia and Lymphoma Society (grant no. 0862-15 (S.-J.D., M.A.D., C.S.T., J.F.S.) and SCOR grant no. 11283-17 (A.W.R., D.C.S.H.)). We thank K. Doig, G. Arnau, T. Semple, T. Holloway and J. Carmody for advice and assistance with genomic sequencing, G. Lessene for providing A-1331852 and the following funders for fellowship, scholarship and grant support: CSL Centenary fellowship (S.-J.D.), Leukaemia Foundation Australia senior fellowship and Howard Hughes Medical Institute international research scholarship 55008729 (M.A.D.), NHMRC postgraduate scholarship 1114242 (R.A.) and HSANZ new investigator fellowship (R.A.), NHMRC fellowships (1089072 (C.E.T.), 1090236 (D.H.D.G.) and 1079560 (A.W.R.), NHMRC grant no. 1104549 (S.-J.D., M.A.D., C.S.T., J.F.S.) and programs 1113577, 1016701 (A.W.R., D.C.S.H.) and Leukemia and Lymphoma Society Independent Research Institutes Infrastructure Support Scheme grant no. 9000220 (R.T.), Snowdome Foundation (M.A.A.), Maddie Riewoldt's Vision 064728 (Y.-C.C.), Victorian State Government Operational Infrastructure Support grant and Cancer Council Victoria grant (nos. 1146518, 1102104) and the Peter MacCallum Cancer Foundation. Mass cytometry was performed in part at the Materials Characterization and Fabrication Platform at the University of Melbourne and the Victorian Node of the Australian National Fabrication Facility, with support from the Victorian Comprehensive Cancer Centre.

Author contributions

R.A. and Y.-C.C. performed the majority of the experiments, helped develop the overall concept behind the analysis, and helped write the manuscript. T.H., D.V., C.E.T., R.T., P.Y., S.Q.W., S.F., E.Y.N.L., M.A.A., C.P., O.G., C.C.B., K.K., P.B., K.R., A.Z., J.L., M.W. and D.H.D.G. contributed to data analysis. D.C.S.H. provided critical reagents. C.S.T., J.F.S. and A.W.R initiated and conducted the AIM clinical trial, provided patient data,

facilitated biospecimen collection and contributed to the interpretation of the research findings. S.-J.D. and M.A.D. developed the overall concept behind the study, supervised the experiments, analyzed the data and wrote the manuscript.

Competing interests

C.E.T., R.T., M.A.A., D.C.S.H., D.H.D.G. and A.W.R. are employees of Walter and Eliza Hall Institute of Medical Research which receives milestone and royalty payments related to venetoclax. C.S.T., J.F.S. and A.W.R. received funding from Janssen and AbbVie to conduct the AIM clinical trial. The remaining authors declare no competing interests.

Additional information

Supplementary information is available for this paper at https://doi.org/10.1038/s41591-018-0243-z.

Correspondence and requests for materials should be addressed to M.A.D. or S.-J.D.

Methods

Patients and sample collections. We carried out a prospective analysis of tumor tissue and whole blood samples collected from patients recruited to the AIM study (NCT02471391). This was an investigator-initiated, open-label, single-arm phase 2 clinical trial, approved by the Peter MacCallum Cancer Centre research ethics committee (14/148). Eligible patients had relapsed/refractory MCL, or, if previously untreated, were unsuitable for DNA-damaging chemotherapy. A total of 24 participants were recruited and all provided written informed consent. Serial CT and/or FDG-PET, BM biopsies and whole blood samples were collected from all enrolled patients at baseline, weeks 4, 16, 28, 40, 56 and at the time of disease progression (Supplementary Tables 1 and 2). Fresh or archival tumor tissue was available in all cases at baseline before treatment ($n=24$), and additional tumor biopsies were also performed where possible at disease progression in patients with acquired resistance ($n=2$; lymph node biopsy in patient 07 and pleural biopsy in patient 01). The primary endpoint of the study was complete response measured using CT, without consideration of PET result, at 16 weeks. This was to allow a historical comparison with patients treated with ibrutinib monotherapy. Samples from a patient treated outside the trial and a normal donor were accessed after informed consent under approvals of the Melbourne Health human research ethics committee (2005.008 and 2016.305).

Sample processing and DNA extraction. Blood was collected in EDTA tubes and processed within 2 h of collection. Whole blood was first centrifuged at 1,600*g* for 10 min to separate the plasma from the peripheral blood cells, followed by a further centrifugation step at 20,000*g* for 10 min to pellet any remaining cells and/or debris. The plasma was then stored at −80 °C until DNA extraction. DNA was extracted from 2-ml aliquots of plasma using the QIAamp Circulating Nucleic Acid kit (Qiagen, 55114) according to manufacturer's instructions. The DNA was then eluted into 50 µl buffer AVE (Qiagen) and stored at −20 °C.

After collection of plasma from each blood sample, the mononuclear cell layer was collected using the Ficoll-Paque Plus (GE Healthcare, 17144002) separation method, according to the manufacturer's protocols. Red cell lysis was performed using a red cell lysis buffer (155 mM NH_4Cl, 10 mM $KHCO_3$ and 0.1 mM EDTA pH 7.4). Mononuclear cell layer cells were then enumerated using a hemocytometer and aliquots of 5×10^6 cells were snap-frozen in liquid nitrogen and stored at −80 °C. BM aspirates were similarly processed by the Ficoll separation method to obtain bone marrow-derived cells. DNA was extracted from the BM or peripheral blood mononuclear cell layer cells using the DNA Blood and Tissue kit (Qiagen, 69504), as per manufacturer's protocols.

DNA from formalin-fixed, paraffin-embedded tissue was extracted using the Qiagen DNeasy Blood and Tissue kit (Qiagen, 69506), according to manufacturer's protocols. DNA from fresh frozen tissue was extracted using the QIAamp DNA FFPE Tissue kit (Qiagen, 56404), according to manufacturer's protocols.

Matched normal DNA was obtained from study participants to enable confirmation of somatic status of identified genetic events. Approximately 2 ml saliva was collected in an Oragene Saliva Collection kit (DNA Genotek, OG500). DNA was then extracted from saliva using the PrepIT L2P kit (DNA Genotek, PTL2P45), according to the manufacturer's protocols. DNA was quantified using a Qubit fluorometer (Invitrogen) and a Quant-iT dsDNA HS kit (Invitrogen).

Identification of somatic genomic alterations. Genomic DNA from tumor and matched normal tissues was subjected to WES and/or targeted amplicon sequencing and LC-WGS (Supplementary Table 2). Candidate mutations identified from WES were validated and confirmed as somatic by targeted amplicon sequencing, designed to cover a panel of 42 genes recurrently mutated in lymphoid malignancies (Supplementary Tables 3 and 5).

To assay circulating DNA carrying specific somatic genomic alterations, we performed direct-targeted amplicon sequencing of plasma DNA (Supplementary Tables 2 and 8). In selected cases, droplet digital PCR, WES and LC-WGS were also performed on plasma DNA (Supplementary Tables 2 and 9).

Targeted amplicon sequencing. Targeted amplicon sequencing was performed using the 48.48 Access Array system (Fluidigm), as described previously[41]. A panel of 226 amplicons with an average size of 170 base pairs (bp) was designed across 42 genes recurrently mutated in lymphomas (see Supplementary Tables 6 and 7 for a full list of genes and primers). Plasma, tumor tissue and germline (saliva) DNA were then amplified with tagged target-specific primers using the microfluidic platform, which allowed 48 samples to be analyzed simultaneously with multiplexed assays in 2,448 reaction chambers. DNA derived from plasma and formalin-fixed, parafin-embedded tissue samples were first subjected to preamplification in a 10 µl reaction volume containing a pool of forward and reverse target-specific primers using the Fast Start High Fidelity PCR System (Roche, 04738292001). The preamplified samples were diluted fivefold in PCR-grade water before target-specific amplification using the Access Array system. DNA from bone marrow aspirates, fresh tissue and germline samples was not preamplified, and 50 ng DNA was used directly for target-specific amplification using the Access Array system. Following amplification, products were collected, tagged with sample-specific barcodes, pooled together and purified using AMPure XP beads. All samples were analyzed in duplicate to control for PCR artifacts. The purified libraries were then sequenced using 150-bp read length on the Illumina MiSeq sequencer. The mean targeted sequencing coverage was 700-fold for plasma, 1,500-fold for tumor and 1,200-fold for matched normal DNA. Sequenced reads were mapped to the human reference genome (version hg19) using BWA-MEM (version 0.7.12) with default parameters.

CASAVA v1.8.2 was used to perform sample demultiplexing and to convert BCL files generated from the MiSeq instrument into FastQ files containing short-read data. Using the primer sequences that are present in the data, short reads were first assigned to their respective amplicon. A global alignment on the basis of a modified Needleman–Wunsch algorithm[42] was then performed between the reads and the hg19-derived amplicon reference sequence. Sequence variants were detected using VarScan 2[43]. Raw variants were then deposited into 'PathOS': an in-house web-based variant management system[44]. Mutations with at least 50× coverage with a minimum of ten reads supporting the variant were retained for further analysis. Variants that were recurrently observed in >50% of the samples (representing probable sequencing and/or PCR artifacts) and those with a high global allele frequency (>1.0%) in the 1,000 genomes database were flagged and removed from this curated list. Variants in the curated list were then annotated on the basis of their prognostic or functional relevance, as described previously[45].

Whole-exome sequencing. WES was performed on tissue, plasma and germline DNA samples ($n=36$; Supplementary Table 2). DNA (150–300 ng) for tissue and germline samples was fragmented to approximately 200 bp using a focal acoustic device (Covaris S2, Sage Sciences). Libraries were prepared with the Kapa Hyper Prep kit (Kapa Biosystems) and SureSelectXT adapters (Agilent). Hybridization capture was performed with SureSelect Human All Exon V6 baits following the SureSelectXT recommended protocol (Agilent). Indexed libraries were sequenced on an Illumina NextSeq500 (Illumina) to generate on average 167 million paired-end 75 bp reads per sample. The mean exome sequencing coverage was 90-fold for plasma, 142-fold for tumor and 132-fold for matched normal DNA.

FASTQ sequences files for each sample were evaluated with FASTQC (version 0.110.3) for quality control and Cutadapt (version 1.8.1) was used to remove adapter sequences, primers and other sequence artifacts. The reads were then mapped to the human reference genome (version hg19) using BWA–MEM (version 0.7.12) with default parameters. PCR duplicates were removed using Picard (version 1.133). Local realignment was performed using GATK (version 3.4.0) IndelRealigner. GATK's BaseRecalibrator was then used for recalibration of base qualities. SAMtools mpileup command was used to create pileup files for variant calling. Single nucleotide variant and indel detection was performed with GATK, VarScan (version 2.3.8) and MuTect (version 1.1.7). Mutations were annotated for read depth of reference and alternate alleles, and Ensembl Variant Effect Predictor (version 80) and COSMIC (version 72) were used to explore the impact of the detected somatic mutations. We retained predicted functional mutations (nonsense, missense, frameshift or splicing single nucleotide variants) for further analysis. All variants with mutant reads observed in the matched normal sample were discarded. Mutations that had strand bias and those detected within homopolymer regions were also removed.

Low-coverage whole-genome sequencing. LC-WGS was performed on DNA from baseline tumor samples ($n=24$), progression tumor samples ($n=2$) and plasma samples ($n=17$). DNA (150–300 ng) for tissue and germline samples was fragmented to approximately 200 bp using a focal acoustic device (Covaris S2, Sage Sciences). Libraries were prepared with NEB-Next Ultra II kit (NEB) according to the manufacturer's instructions. Indexed libraries were sequenced on an Illumina NextSeq500 (Illumina) to generate on average 65 million paired-end 75 bp reads per sample as described previously[46]. The mean LC-WGS coverage was 3.3-fold for plasma and 1.2-fold for tumor. Reads were aligned to the hg19 genome using BWA (version 0.7.13), resulting in an average mapping rate of 97.5% per sample. Copy number analysis was performed using QDNASeq (version 1.12.0). The genome was divided into nonoverlapping 1-kilobase (kb) or 15-kb bins, and the number of reads mapping within each bin was counted and adjusted with a simultaneous 2D locally estimated scatterplot smoothing (LOESS) correction accounting for read mappability and GC content[47]. All other QDNASeq parameters were set as default. Copy number changes were reported as transformed absolute copy number values ($\log_2$(absolute copy number) − 1). Thus, diploid regions were reported as 0. The threshold utilized for calling amplifications was transformed copy number > 1, corresponding to >4 copies. The threshold utilized for calling deletions was transformed copy number < −0.6, corresponding to a ~35% copy number loss.

The segmented copy number calls from (i) baseline tumor DNA of responders and nonresponders, or (ii) baseline plasma DNA of responders and nonresponders were used as input for GISTIC (version 2.0.23) analysis[32]. Both the GISTIC *G* score, which considers the amplitude of the copy number change as well as its frequency across samples, and the false discovery rate (FDR)-adjusted *q* value were considered when defining significant copy number changes. For baseline tumor samples, a *G* score threshold of 1 and an FDR-adjusted *q* value threshold of 0.25 were applied. For plasma samples, an identical *G* score threshold and a higher *q* value threshold of 0.5 were applied as the tumor fraction was lower in plasma samples due to the high fraction of cell-free DNA compared with ctDNA.

Droplet digital PCR. Droplet digital PCR was performed using the BioRad QX200 droplet digital PCR system following manufacturer's protocols. Allele-specific PCR assays to specifically detect and quantify the fractional abundance of point mutations and corresponding wild type alleles were commercially obtained (PrimePCR PCR Primers and Assays, BioRad Laboratories) (Supplementary Table 9). The total amount of cell-free DNA was quantified using an assay that targets a nonamplified region in the genome, the *RPP30* gene on chromosome 10, as described previously[41]. Each sample was analyzed by at least two technical replicates. A Poisson correction was applied to determine the number of amplifiable molecules, which was used to further derive the number of copies of DNA carrying a particular mutation per ml of plasma. Data analysis was carried out using the QuantaSoft Software, version 1.7 (BioRad).

MRD analysis. MRD was quantified by eight-color flow cytometry of the bone marrow (minimum sensitivity of 10^{-3} to 10^{-4}, depending on the number of available events) and by ASO–PCR (targeting either the clonal IgH rearrangement or the t(11;14) translocation designed to reach a sensitivity of 10^{-5}) in blood. ASO–PCR was performed and reported in accordance with EuroMRD guidelines[23].

FISH analysis. Slides were deparaffinised twice in xylene for 5 min, rehydrated twice in 100% and then 70% ethanol and washed in distilled water for 2 min each. Slides in 70 ml heat pretreatment solution (SPoT-Light Tissue Pretreatment Kit, Life Technologies) were placed under high pressure for 2 min, left to cool for 30 min and rinsed in distilled water. Enzyme reagent (SPoT-Light Tissue Pre-treatment Kit, Life Technologies) was added and the slides were incubated for 30 min in a humidified chamber, washed in distilled water, run through an ethanol series (70%, 80% and 100%) for 1 min each and air dried. Slides were co-denatured with the XL CDKN2A Deletion Probe (Metasystems) at 85 °C for 5 min and hybridized overnight in a humidified chamber at 37 °C. They were then washed in 2× SSC/0.1% NP-40 at 73 °C for 2 min, air dried and cover slipped with DAPI (10 mg ml^{-1}).

Cell culture. The human MCL cell lines Z-138 and Granta-519 were obtained from ATCC and authenticated by short-tandem-repeat profiling through the Victorian Centre for Functional Genomics. Z-138 and Granta-519 cells were regularly tested and verified to be mycoplasma negative by PCR analysis by the Victorian Infectious Diseases References Laboratory. The Z-138 cell line was grown in IMDM with 10% FBS (Life Technologies) and incubated at 37 °C, 5% CO_2. The Granta-519 cell line was grown in DMEM with 10% FBS (Life Technologies) and incubated at 37 °C, 5% CO_2.

RNA interference. Z-138 and Granta-519 cells were transduced with inducible shRNA expression vectors; TtRMPVIR (Addgene, 27995), or constitutive shRNA expression vector; pGIPZ, and cells expressing shRNA were sorted by flow cytometry as previously described[48]. Knockdown efficiency of shRNA-expressing and non-shRNA-containing cells was assessed after 48–72 h of doxycycline exposure by qRT–PCR and immunoblotting.

shRNA sequences. Sequences for shRNAs (with targets in parentheses) were as follows: shSCR (scramble), 5′-ATCTCGCTTGGGCGAGAGTAAG-3′; SM4 (*SMARCA4*), 5′-CAGAAGAAATCATCACGGA-3′; SM4-2 (*SMARCA4*), 5′-AG CCTCAACGACCTAGAGA-3′; ATF3 (*ATF3*), 5′-GGGTTGTGCTTTCTAGCA A-3′; ATF3-2 (*ATF3*), 5′-AAGAGGCGACGAGAAAGAA-3′.

Competition assay. Wild-type Z-138 and shRNA-containing Z-138 cells were recombined at a 1:1 ratio and seeded at a density of 1×10^5 cells per well in 24-well plates. For drug treatment, 3 μM venetoclax[49], 3 μM ibrutinib, 100 nM A-1331852[50] or 50 nM navitoclax and 1 μg ml^{-1} of doxycycline final concentrations were added to each well or in combination; as a control DMSO of equivalent volume was used. Every 2 d, cells were sampled and analyzed for cell viability using DAPI exclusion and for the proportion of shRNA-expressing (dsRED/Venus) cells using BD LSR II. The flow cytometry gating strategy is shown in Supplementary Fig. 10.

Cell proliferation and viability assays. Z-138 and Granta-519 cells were seeded at a density of 5×10^4 per well in 24-well plates. Cells were cultured in the presence of drugs or equivalent DMSO concentrations. For single treatments, venetoclax and ibrutinib were used at 1, 3 and 5 μM each. Venetoclax and ibrutinib were used at a final concentration of 3 μM each when used together, A-1331852 was used at a 100 nM, navitoclax was used at 50 nM, or in combination for Z-138. Venetoclax and ibrutinib were used with a final concentration of 1 and 3 μM, respectively, for Granta-519 cells. Every 2 to 3 d, cells were sampled and analyzed for cell viability by DAPI exclusion and cell numbers were measured using BD FACSVerse. For apoptosis assays, annexin-V stain was added to cells (1:50) and incubated for 30 min before analysis by flow cytometry. The flow cytometry gating strategy is shown in Supplementary Fig. 10.

For primary cells, peripheral blood mononuclear cells from the patient with MCL at progression on venetoclax after prior progression on ibrutinib were thawed and seeded in 96-well plates at 100,000 cells per well. Five-point 1:8 serial dilutions of compounds starting from 10 μM were used for the screen. Cell viability was assessed at 24 h for venetoclax, ABT-737, A-1331852 and ibrutinib using a FACSFortessa (Becton Dickinson) flow cytometer to determine cell viability by propidium iodide exclusion. FACS data were analyzed using FlowJo software. The flow cytometry gating strategy is shown in Supplementary Fig. 10.

qRT–PCR. mRNA was prepared using the Qiagen RNeasy kit, and cDNA synthesis was performed using SuperScript VILO kit (Life Technologies) as per manufacturer's instructions. qPCR analysis was performed on an Applied Biosystems StepOnePlus System with SYBR green reagents (Life Technologies). For analysis of cell line samples, expression levels were determined using the discrete cosine transform method and normalized to β-2-microglobulin (B2M) and/or GADPH.

qRT–PCR primer sequences. qRT–PCR primer sequences were as follows: SMARCA4, 5′-AGATGCACAAGCCCATGGAGTC-3′ (forward) and 5′-CTGGACTAGAGGCATGCTCAG-3′ (reverse); Bcl-xL, 5′-GATCCCCATGGCAGCAGTAAAGCAAG-3′ (forward) and 5′-CCCCATCCCGGAAGAGTTCATTCACT-3′ (reverse); B2M, 5′-TGACTTTGTCACAGCCCAAG-3′ (forward) and 5′-AGCAAGCAAGCAGAATTTGG-3′ (reverse); GAPDH, 5′-ACAGGGCACTGTAGGCAGAT-3′ (forward) and 5′-TGGACTCCACGACGTACTCA-3′ (reverse); ATF3, 5′-CTGGAATCAGTCACTGTCA-3′ (forward) and 5′-CTTCTCCGACTCTTTCTG-3′ (reverse).

Immunoblotting. Whole-cell lysates were mixed with Laemmli SDS sample buffer with complete protease inhibitors (Roche), separated via SDS–PAGE and transferred to PVDF or nitrocellulose membranes (Millipore). Membranes were then sequentially incubated with primary antibodies and secondary antibodies conjugated with horseradish peroxidase (Invitrogen). Membranes were then incubated with ECL (GE Healthcare) and proteins detected by exposure to X-ray film. The following antibodies were used in immunoblotting assays: Brg-1/SMARCA4 (G-7): sc-17796 (lot no. K3016), HSP 60 (C-10): sc-376240 (lot no. H1413), ATF3 (c-19): sc-188, ATF3 (44C3a): sc-81189, BCL2 (BCL2-100, WEHI), Bcl-xL (clone 10112; BD Biosciences), and HSP70 (clone N6; WEHI).

RNA sequencing. Control or SMARCA4 knockdown Z-138 cells treated with 3 μM venetoclax and 3 μM ibrutinib or equivalent volume of DMSO for 8 h were analyzed in three biological replicates. The cells were mixed with *Drosophila* S2 cells at a ratio of 19:1. RNA for RNA-seq was isolated from the mixed human and *Drosophila* using the Qiagen RNeasy kit. RNA concentration was quantified with the NanoDrop spectrophotometer (Thermo Scientific). The RNA integrity was assessed with the Agilent TapeStation using the RNA ScreenTape. Libraries were prepared using the lexogen QuantSeq 3' mRNA-Seq Library Prep Kit. Libraries were quantified by qPCR, normalized and pooled to 2 nM before sequencing with single-end 75-bp reads on an Illumina NextSeq500.

Reads were aligned to the human genome (G1k V37) using HiSAT2[51], and reads were assigned to genes using htseq-count[52]. Differential expression was calculated using edgeR[53]. Genes with a false discovery rate corrected for multiple testing using the method of Benjamini and Hochberg below 0.05 and a fold-change greater than 2 were considered significantly differentially expressed. Principal component analysis was performed on the RNA-seq data.

Chromatin immunoprecipitation. Z-138 cells were crosslinked with 1% formaldehyde for 15 min at room temperature, and crosslinking was stopped by the addition of 0.125 M glycine. Cells were then lysed in 1% SDS, 10 mM EDTA, 50 mM Tris-HCl, pH 8.0 and protease inhibitors. Lysates were sonicated in a Covaris ultrasonicator to achieve a mean DNA fragment size of 500 bp. Immunoprecipitation with anti-Histone H3 (acetyl K27) antibody (ab4729) was performed for a minimum of 12 h at 4 °C in modified RIPA buffer (1% Triton X-100, 0.1% deoxycholate, 90 mM NaCl, 10 mM Tris-HCl, pH 8.0 and protease inhibitors). Equal volumes of protein A and G magnetic beads (Life Technologies) were used to bind the antibody and associated chromatin. Reverse crosslinking of DNA was followed by DNA purification with QIAquick PCR purification kits (Qiagen). PCR was performed in the *Bcl-xL* region with the following primers: 5′- CATATGAGGCAACAGGCAGA-3′ (forward) and 5′- ATGCCTGGCACA CAGTAGGT-3′ (reverse).

Z-138 H3K27ac ChIP data were downloaded from a publicly available dataset (ERX926128). Reads were aligned to the human genome (G1k V37) with BWA–MEM[54]. Peak calling was performed with MACS2[55] with default parameters. Genome browser images of ChIP-seq data were generated by converting the bam files from BWA to TDF files with igvtools and viewing in IGV[56]. ChIP-seq coverage across selected genomic regions was calculated with BEDtools[57].

ATAC-seq. Z-138 cells were washed with ice-cold PBS, then lysed in 500 μl lysis buffer (10 mM Tris-HCl pH 7.4, 10 mM NaCl, 3 mM $MgCl_2$, 0.1% NP-40). After centrifugation, the cell pellet was resuspended in 50 μl of tagmentation

mastermix (1× TD buffer, 0.01% digitonin and 2.5 µl transposase) from the Nextera DNA library prep kit (Illumina) and incubated at 37 °C for 30 min. The tagmented chromatin was purified with the MinElute PCR purification kit (Qiagen) and then amplified for 13 PCR cycles with the forward and reverse Indexing primers (25 µM) and HotStart KAPA readymix. The PCR products were purified with the MinElute PCR purification kit (Qiagen), then analyzed with the Agilent TapeStation using the D1000 ScreenTape to assess the size of library fragments. ATAC-seq libraries were quantified by qPCR, normalized and pooled to 2 nM before sequencing with paired-end 75-bp reads on an Illumina NextSeq500.

Mass cytometry. Peripheral blood mononuclear cells from the patients with MCL were obtained after Ficoll density gradient centrifugation. Cells at the interphase were collected, washed twice in HBSS supplemented with 5% fetal calf serum and 2.5% 1 M Tris pH 7. Cells were frozen in Iscove modified Dulbecco medium supplemented with 15% fetal calf serum and 10% DMSO and stored in liquid nitrogen.

Cells from the patients and MCL cell line Z-138 were thawed and stained for viability with cisplatin. Cells were then fixed with paraformaldehyde (PFA, Electron Microscopy Sciences) to a final concentration of 1.6% for 10 min at room temperature. Cells were pelleted and washed once with cell-staining medium (CSM, PBS with 0.5% BSA and 0.02% sodium azide) to remove residual PFA and then were stored at −80 °C.

Cells were barcoded using 20-plex palladium barcoding according to the manufacturer's instructions (Fluidigm). Following barcoding, cells were pelleted and washed once with CSM (PBS with 0.5% BSA and 0.02% sodium azide) to remove residual PFA. Cells were permeabilized with 4 °C methanol for 10 min. Cells were washed three times with CSM and stained with anti-BCL2 ^{157}Gd (clone 100, WEHI) and anti-Bcl-xL ^{153}Eu (Clone E18, Abcam) for 30 min at room temperature. Cells were washed with CSM and then stained with 125 nm ^{191}Ir/^{193}Ir DNA intercalator (Fluidigm) in PBS with 1.6% PFA at 4 °C overnight. Cells were washed once with CSM, washed three times with double-distilled water, filtered to remove aggregates and resuspended with EQ normalization beads immediately before analysis using a Helios mass cytometer (Fluidigm). Throughout the analysis, cells were maintained at 4 °C and introduced at a constant rate of ~300 cells per second.

Data concatenation, normalization and debarcoding were done in the Helios software, version 6.7.1014 (Fluidigm). Single cells were gated using the Flowjo (version 10.4) and Cytobank software (http://www.cytobank.org) based on event length and ^{191}Ir/^{193}Ir DNA contents to avoid debris and doublets.

Statistics and reproducibility. Statistical significance was determined using Fisher's *t*-test. Survival analyses were performed using the Cox's proportional hazards model. For patient groups with no events, Cox regression with Firth's penalized likelihood were used to estimate significance and hazard ratios[58]. Computation was done using R packages 'survival' and 'coxphf.' For all experiments, statistical methods are noted in the figure and table legends.

Reporting Summary. Further information on research design is available in the Nature Research Reporting Summary linked to this article.

Data availability

The data that support the findings of this study are available from the corresponding author upon request. The sequencing data that supports the findings of this study has been deposited into the sequence read archive, which is hosted by the National Centre for Biotechnology Information. The BioProject accession number is PRJNA489753.

References

41. Dawson, S. J. et al. Analysis of circulating tumor DNA to monitor metastatic breast cancer. *N. Engl. J. Med.* **368**, 1199–1209 (2013).
42. Needleman, S. B. & Wunsch, C. D. A general method applicable to the search for similarities in the amino acid sequence of two proteins. *J. Mol. Biol.* **48**, 443–453 (1970).
43. Koboldt, D. C. et al. VarScan 2: somatic mutation and copy number alteration discovery in cancer by exome sequencing. *Genome Res.* **22**, 568–576 (2012).
44. Doig, K. D. et al. PathOS: a decision support system for reporting high throughput sequencing of cancers in clinical diagnostic laboratories. *Genome Med.* **9**, 38 (2017).
45. Wong, S. Q. et al. Assessing the clinical value of targeted massively parallel sequencing in a longitudinal, prospective population-based study of cancer patients. *Br. J. Cancer* **112**, 1411–1420 (2015).
46. Wong, S. Q. et al. UV-associated mutations underlie the etiology of MCV-negative Merkel cell carcinomas. *Cancer Res.* **75**, 5228–5234 (2015).
47. Scheinin, I. et al. DNA copy number analysis of fresh and formalin-fixed specimens by shallow whole-genome sequencing with identification and exclusion of problematic regions in the genome assembly. *Genome Res.* **24**, 2022–2032 (2014).
48. Fong, C. Y. et al. BET inhibitor resistance emerges from leukaemia stem cells. *Nature* **525**, 538–542 (2015).
49. Anderson, M. A. et al. The BCL2 selective inhibitor venetoclax induces rapid onset apoptosis of CLL cells in patients via a TP53-independent mechanism. *Blood* **127**, 3215–3224 (2016).
50. Leverson, J. D. et al. Exploiting selective BCL-2 family inhibitors to dissect cell survival dependencies and define improved strategies for cancer therapy. *Sci. Transl. Med.* **7**, 279ra240 (2015).
51. Kim, D., Langmead, B. & Salzberg, S. L. HISAT: a fast spliced aligner with low memory requirements. *Nat. Methods* **12**, 357–360 (2015).
52. Anders, S., Pyl, P. T. & Huber, W. HTSeq—a Python framework to work with high-throughput sequencing data. *Bioinformatics* **31**, 166–169 (2015).
53. Robinson, M. D., McCarthy, D. J. & Smyth, G. K. edgeR: a Bioconductor package for differential expression analysis of digital gene expression data. *Bioinformatics* **26**, 139–140 (2010).
54. Li, H. & Durbin, R. Fast and accurate short read alignment with Burrows–Wheeler transform. *Bioinformatics* **25**, 1754–1760 (2009).
55. Zhang, Y. et al. Model-based analysis of ChIP-Seq (MACS). *Genome Biol.* **9**, R137 (2008).
56. Robinson, J. T. et al. Integrative genomics viewer. *Nat. Biotechnol.* **29**, 24–26 (2011).
57. Quinlan, A. R. & Hall, I. M. BEDTools: a flexible suite of utilities for comparing genomic features. *Bioinformatics* **26**, 841–842 (2010).
58. Heinze, G. & Schemper, M. A solution to the problem of monotone likelihood in Cox regression. *Biometrics* **57**, 114–119 (2001).

nature research

Corresponding author(s): Mark Dawson and Sarah-Jane Dawson

Reporting Summary

Nature Research wishes to improve the reproducibility of the work that we publish. This form provides structure for consistency and transparency in reporting. For further information on Nature Research policies, see Authors & Referees and the Editorial Policy Checklist.

Statistical parameters

When statistical analyses are reported, confirm that the following items are present in the relevant location (e.g. figure legend, table legend, main text, or Methods section).

n/a	Confirmed	
☐	☒	The exact sample size (*n*) for each experimental group/condition, given as a discrete number and unit of measurement
☐	☒	An indication of whether measurements were taken from distinct samples or whether the same sample was measured repeatedly
☐	☒	The statistical test(s) used AND whether they are one- or two-sided *Only common tests should be described solely by name; describe more complex techniques in the Methods section.*
☐	☒	A description of all covariates tested
☐	☒	A description of any assumptions or corrections, such as tests of normality and adjustment for multiple comparisons
☐	☒	A full description of the statistics including central tendency (e.g. means) or other basic estimates (e.g. regression coefficient) AND variation (e.g. standard deviation) or associated estimates of uncertainty (e.g. confidence intervals)
☐	☒	For null hypothesis testing, the test statistic (e.g. *F*, *t*, *r*) with confidence intervals, effect sizes, degrees of freedom and *P* value noted *Give P values as exact values whenever suitable.*
☒	☐	For Bayesian analysis, information on the choice of priors and Markov chain Monte Carlo settings
☒	☐	For hierarchical and complex designs, identification of the appropriate level for tests and full reporting of outcomes
☒	☐	Estimates of effect sizes (e.g. Cohen's *d*, Pearson's *r*), indicating how they were calculated
☐	☒	Clearly defined error bars *State explicitly what error bars represent (e.g. SD, SE, CI)*

Our web collection on statistics for biologists may be useful.

Software and code

Policy information about availability of computer code

Data collection	Flow cytometry data was collected using LSR II, FACSVERSE, FACSFortessa X20 (BD Biosciences); Sequencing data was collected using MiSeq, Next-Seq500 (Illumina); Droplet digital data was collected using Droplet Digital PCR system (Bio-Rad); Quantative PCR data was collected using StepOnePlus Real-Time PCR system (Applied Biosystems); Mass cytometry data was collected using Helios mass cytometer (Fluidigm)
Data analysis	BD FACSuite (BD Biosciences), FlowJo V10, and FlowLogic 7 (Inivai) software were used to collect and analyze flow cytometry data. In house designed and previously validated bioinformatic pipelines were used to analyse targeted amplicon and whole exome sequencing data. QDNAeq (v1.12.0) and GISTIC (v2.0.23) was used to analyse whole genome sequencing data. Limma (v3.34.9) and edgeR (v3.20.9) was used to analyse RNA sequencing data. Ngsplot (v2.61) and macs2 (v2.1.1) were used to analyse ATAC and ChIP sequencing data. QuantaSoft software v1.7 (Bio-Rad) was used to interpret digital PCR data. StepOnePlus (Applied Biosystems) software was used to analyse quantitative PCR data. Helios (Fluidigm) and Cytobank (www.cytobank.org) software were used to analyse mass cytometry data. Statistical analysis was performed using R or Prism 7 (GraphPad)

For manuscripts utilizing custom algorithms or software that are central to the research but not yet described in published literature, software must be made available to editors/reviewers upon request. We strongly encourage code deposition in a community repository (e.g. GitHub). See the Nature Research guidelines for submitting code & software for further information.

Data

Policy information about availability of data

All manuscripts must include a data availability statement. This statement should provide the following information, where applicable:

- Accession codes, unique identifiers, or web links for publicly available datasets
- A list of figures that have associated raw data
- A description of any restrictions on data availability

The sequencing data that support the findings of this study has been deposited into the sequence read archive, which is hosted by the National Centre for Biotechnology Information. The BioProject accession number is PRJNA489753

Field-specific reporting

Please select the best fit for your research. If you are not sure, read the appropriate sections before making your selection.

☒ Life sciences ☐ Behavioural & social sciences ☐ Ecological, evolutionary & environmental sciences

For a reference copy of the document with all sections, see nature.com/authors/policies/ReportingSummary-flat.pdf

Life sciences study design

All studies must disclose on these points even when the disclosure is negative.

Sample size	The sample size of 24 patients used in the study was determined by the AIM clinical trial (Tam C.S., et. al. N Engl J Med 2018; 378:1211-1223)
Data exclusions	No data was excluded from the study
Replication	Experimental data was replicated in at least triplicate unless otherwise stated in the manuscript and all replicated experiments were successful
Randomization	This was not a randomized study, as per the AIM clinical trial (Tam C.S., et. al. N Engl J Med 2018; 378:1211-1223)
Blinding	Blind data and stats analysis was performed

Reporting for specific materials, systems and methods

Materials & experimental systems

n/a	Involved in the study
☒	☐ Unique biological materials
☐	☒ Antibodies
☐	☒ Eukaryotic cell lines
☒	☐ Palaeontology
☒	☐ Animals and other organisms
☐	☒ Human research participants

Methods

n/a	Involved in the study
☒	☐ ChIP-seq
☐	☒ Flow cytometry
☒	☐ MRI-based neuroimaging

Antibodies

Antibodies used	Western blotting : Brg-1 (clone G-7, sc-17796, lot K3016, 1:1000; Santa Cruz); HSP 60 (clone C-10, sc-376240, lot H1413, 1:1000; Santa Cruz); BCL-2 (BCL2-100, 1:500; WEHI); Bcl-xL (cat no. 10112, lot 10112, 1:500; BD Biosciences); HSP70 (clone N6, 1:5000; WEHI). Mass cytometry: BCL-2 157Gd (clone 100, 2ug/mL; WEHI); Bcl-xL 153Eu (Clone E18, 2ug/mL; Abcam). ChIP: anti-Histone H3(acetyl K27) antibody (ab4729, lot GR244014-1, 5ug/assay; Abcam)
Validation	All antibodies were validated as described on the manufactures website, and relevant citations are also listed there

Eukaryotic cell lines

Policy information about cell lines

Cell line source(s)	Z-138 and GRANTA-519 mantle cell lines used in this study were purchased from ATCC
Authentication	authenticated by STR profiling by the Victorian Centre for Functional Genomics centre
Mycoplasma contamination	All cell lines used are mycoplasma negative as tested by the Victorian Infectious Diseases References Laboratory
Commonly misidentified lines (See ICLAC register)	No commonly misidentified cell lines were used

Human research participants

Policy information about studies involving human research participants

Population characteristics	The population characteristics of patients on AIM clinical trial have previously been reported and can be found in Tam C.S., et. al. N Engl J Med 2018; 378:1211-1223.
Recruitment	Patients were recruited in AIM study based on well defined inclusion criteria that were decided and approved before the conduct of study

Flow Cytometry

Plots

Confirm that:

☒ The axis labels state the marker and fluorochrome used (e.g. CD4-FITC).

☒ The axis scales are clearly visible. Include numbers along axes only for bottom left plot of group (a 'group' is an analysis of identical markers).

☒ All plots are contour plots with outliers or pseudocolor plots.

☒ A numerical value for number of cells or percentage (with statistics) is provided.

Methodology

Sample preparation	Cultured cell lines and peripheral blood mononuclear cells from patient
Instrument	FACSVERSE, FACSFortessa, LSR II (BD Bioscience)
Software	FACSuite (BD Bioscience), FlowJo and FlowLogic (Inivai) software was used to collect and analyze data
Cell population abundance	Not applicable
Gating strategy	FSC-A and FSC-H was used to identify single cells. Single cells were then gated for morphology by SSC-A and FSC-A. Cell with the correct morphology separated by viability using DAPI or PI exclusion (plus AnnexinV for apoptosis assay) and intrinsic GFP and dsRED expression

☒ Tick this box to confirm that a figure exemplifying the gating strategy is provided in the Supplementary Information.